

Progress of Theoretical Physics, Vol. 0, No. 0, April 2012

Massive Star Evolution and Nucleosynthesis

— *Lower End of Fe-Core Collapse Supernova Progenitors and
Remnant Neutron Star Mass Distribution* —

Hideyuki UMEDA,¹ Takashi YOSHIDA,¹ and Koh TAKAHASHI¹

¹ *Department of Astronomy, Graduate School of Science, University of Tokyo,
Tokyo 113-0033, Japan*

(Received April , 2012; revised , 2012)

In order to explore various aspects of stellar evolution, supernovae, gamma ray bursts and nucleosynthesis, we have developed a new efficient stellar evolution code. In this paper we describe this new code and compare the results with the ones calculated by the previous code. Specifically we focus on the progenitor evolution of lower end of the Fe-core collapse supernovae, and mass distribution of remnant neutron stars. We describe how different assumptions will lead different neutron star mass distribution. We also review recent works of our research group.

§1. Introduction

Massive stars end their life as supernovae leaving neutron stars behind, or by forming blackholes without explosions if they are not rotating. The critical initial stellar mass for the blackhole formation is usually considered to be about 20 to 25 M_{\odot} but it is uncertain.¹⁾ This is because explosion mechanism for supernovae is not yet known definitely,^{2),3),4),5),6),7)} and also there are still uncertainties in the progenitor models.

Lower end for the neutron star forming supernova is also still uncertain (e.g., Ref. 8)). Here, the uncertainties in the stellar evolution theory may be even larger. It is well known that the stars above around 10 M_{\odot} stars form an Fe core in the end of their evolution. The formation of Fe core is relatively simple for a $M > 13M_{\odot}$ star (review in Ref. 9)). In such a star the hottest region is the center mostly all the time through the evolution. Therefore, heaviest element is synthesized around the center, forming Fe-core in the end.

On the other hand the evolution of $M \lesssim 13M_{\odot}$ stars are more complicated. Less massive stars tend to have temperature inversion between the center and outside regions. This phenomenon is well known for intermediate mass stars with $M < 8M_{\odot}$ after carbon burning, for which the carbon burning starts at off center (e.g., Ref. 10)). For a $M \lesssim 11M_{\odot}$ star, off center O- and/or Si-burning occurs. The off-center burning front propagates inward through complicated burning stages, forming an Fe core eventually. This off center burning becomes sometimes very violent and it could cause some mass ejection^{11),12)} (see also Section 3.1 in this paper). However, such calculations have not been done recently with updated input physics, so it is currently not clear if such mass ejection really occurs.

For less massive stars which do not ignite Ne even at off center, a cool degenerate

O-Ne core is first formed. This O-Ne core grows in mass gradually when the star is in a super AGB phase. Depending on the mass loss rate this O-Ne core reaches the critical mass for core-collapse owing to electron capture.^{13),8)} It is considered that such a star explodes by the neutrino energy transport mechanism.¹⁴⁾

Calculations for the progenitors of such low mass core-collapse supernovae with updated input physics are interesting and important. However, their evolution can be quite different if the initial mass is only slightly different, say by 0.01-0.1 M_{\odot} (e.g., Ref. 8); see also Sec. 3.1). To understand the whole story in this mass range, therefore, we need to calculate stellar evolution in very fine mass grids. This will be quite time consuming and thus currently well-used progenitor models in the literature (e.g., Refs. 12), 15), 16), 17), 18), 19)) do not fully deal with this mass range.

To tackle this problem, we have developed a stellar evolution code for efficient computation. In this paper we describe this new code, the Yoshida-Umeda (YU) code,²⁰⁾ and compare the results with the ones calculated by one of the author, H.U., using the Umeda-Nomoto (UN) code.^{16), 17), 21), 22)} We also briefly review some of the recent works using the YU code and other works in our research group.

This paper is organized as follows. In §2, we describe the new stellar evolution code and differences with previous codes. In §3, massive star evolutions calculated with this code are compared with the ones with a previous code. In this section we also describe the progenitor evolution of lower end of Fe-core collapse SNe in some detail. §4 describes nucleosynthetic aspects including some reviews of our recent works. In §5 remnant neutron star masses are given as a function of progenitor mass. We describe how the different assumption will lead different neutron star mass distribution. §6 reviews other recent works of our research group and §7 gives discussions and Future Prospects.

§2. Stellar evolution code

2.1. Umeda-Nomoto (UN) code

Before describing the YU code, we briefly describe the UN code because we will compare the results of these codes. This code is mostly based on Nomoto-Hashimoto (NH) code¹²⁾ and Saio-Nomoto-Kato (SNK) code.²³⁾ In the UN code, input physics such as equation of state (EOS) are same as the NH code except updates of radiative opacity, neutrino emissivity and electron capture rates.

There are several differences in the NH and SNK codes:

- i) The NH code is a He-star code, which means that it cannot solve stellar atmosphere and hydrogen burning phase. Thus it cannot provide stellar radius correctly. On the other hand, the SNK code solves atmosphere.
- ii) Since the SNK code is not designed for calculating later evolutionary stages of massive stars, it does not deal with nuclear burning after carbon burning stages. Also because of that, the SNK code does not include the acceleration term²⁴⁾ and omit the inertial term in the equation of motion, while the NH code can include it. This acceleration term becomes important for constructing supernova progenitor models just before iron-core collapse.

iii) The treatment of convection is different. Both codes adopt Schwarzschild criterion for convection but the way of mixing is different. The NH code assumes instantaneous mixing in convective regions, while in the SNK code matter is mixed diffusively using the formalism of Ref. 25) taking into account of the semi-convection effects. The energy transfer in a convective region is also different. In the NH code time-dependent mixing length theory^{26),27)} can be included for convective energy transfer, though this effect is not so important for the massive star evolution forming an Fe-core.

In the UN code atmosphere is calculated as the SNK code, the acceleration term is included and the formalism of Ref. 25) is adopted for convective mixing. Convective energy transfer is treated as same as the NH code.

The UN code differs from the NH and SNK codes in the calculations of nucleosynthesis and nuclear energy generation. The NH code assumes *quasi nuclear statistical equilibrium* during the Si burning while the UN code solves full nuclear reaction networks below $\log T(\text{K}) \lesssim 9.6$. Above that temperature both codes assume *nuclear statistical equilibrium* (NSE). In order to calculate nuclear energy generation rates, in the UN code nuclear reaction networks are solved simultaneously with Henyey relaxation, while in the NH and SNK codes abundance is fixed during Henyey relaxation. In this sense the UN code solves abundance implicitly, while the NH and SNK codes solve explicitly. Solving abundance implicitly is the best way to obtain consistency in the energy generation rates and the abundance evolution. However, this has a disadvantage in efficient calculations because solving large reaction networks involves time consuming matrix inversion calculations.

2.2. Yoshida & Umeda (YU) code

Basic structure of this code is based on the SNK code.²³⁾ As mentioned above, although the UN code has been successfully used for the progenitor calculations, it has an disadvantage in the calculation time. To finish a calculation from ZAMS to Fe-core collapse it typically takes few months. Therefore this code is not suitable for a large parameter search. Hence, we have developed a new more efficient code (YU code). Main difference of the YU code from the UN code is the calculations of nucleosynthesis and energy generation.

The YU code solves a full nuclear reaction network from hydrogen burning up to $\log_{10} T_{\text{C}} \sim 10.0$. The nuclear reaction network consists of ~ 300 species of nuclei from n , p to Br. NSE is not assumed in calculations. On the other hand, the nucleosynthesis is solved before Henyey relaxation in the YU code similar to the SNK code. Using the abundance of the next step, the energy generation is calculated during the Henyey relaxation. Therefore, smaller time step is required.

After carbon burning stage, the time interval is typically determined to satisfy the conditions $\Delta \log_{10} T / \log_{10} T \leq 0.001$ and $\Delta \log_{10} \rho / \log_{10} \rho \leq 0.003$ for each mass coordinate. This treatment requires more calculation steps but still saves the calculation time especially in the late phase of the evolution. With this code, we can calculate one model typically in 1 – 2 weeks for massive star evolutions.

This code at present has not implemented the acceleration term yet. We will include that term in near future.

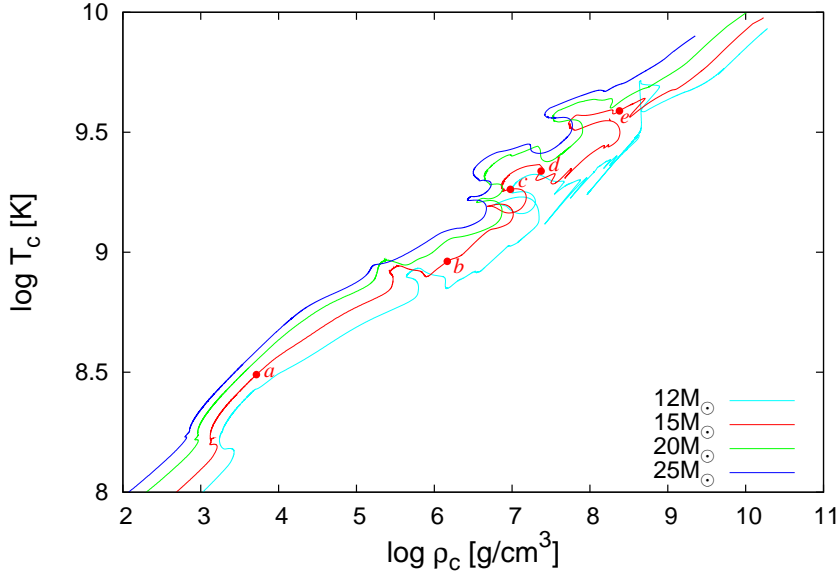


Fig. 1. Evolution tracks of $M = 12, 15, 20$, and $25M_{\odot}$ stars in terms of central temperature and density. Mass fraction distributions of a $15M_{\odot}$ star denoted at the points $a - e$ are shown in Fig. 2.

2.3. Mass loss rates

In the UN and YU codes, same mass loss rates are used for the solar metallicity before the Wolf-Rayet star phases shown in this paper. In OB stars, where the surface temperature is larger than 1.2×10^4 K and the surface H mass fraction is larger than 0.4, the mass loss rate is adopted from Ref. 28). In yellow supergiants and red-giant branches, the mass loss rate in Ref. 29) is used. In the UN code, metallicity dependent factor of $(Z/0.02)^{0.5}$ is multiplied to the rate for metal poor stars as Ref. 30). The YU code adopts the metallicity dependence in a different manner. The metallicity dependence in the main-sequence stage is taken from Ref. 28). In the YU code presented in this paper the case A mass loss rate in the Ref. 20) is used. In yellow supergiants and red-giant branches, the metallicity dependent factor $(Z/0.02)^{0.64}$ is multiplied to the mass loss rate. The power index is the same as that of B supergiants in Ref. 28). See Ref. 20) for the detail.

§3. Progenitor Evolution

Basic properties of massive star evolution have been discussed in many papers (e.g., Refs. 12), 16), 17), 18), 19)), therefore we do not repeat detail here, except $M \simeq 10 - 13M_{\odot}$ models in the next subsection. We briefly describe the evolution in advanced stages of a $M = 15M_{\odot}$ star as an example. Fig. 1 shows the evolution tracks of $M = 12, 15, 20$, and $25M_{\odot}$ stars in terms of the central density and temperature. We also show the mass fraction distributions of the $15M_{\odot}$ star at five stages during the evolution in Fig. 2. Fig. 2(a) indicates the mass fraction distribution after the

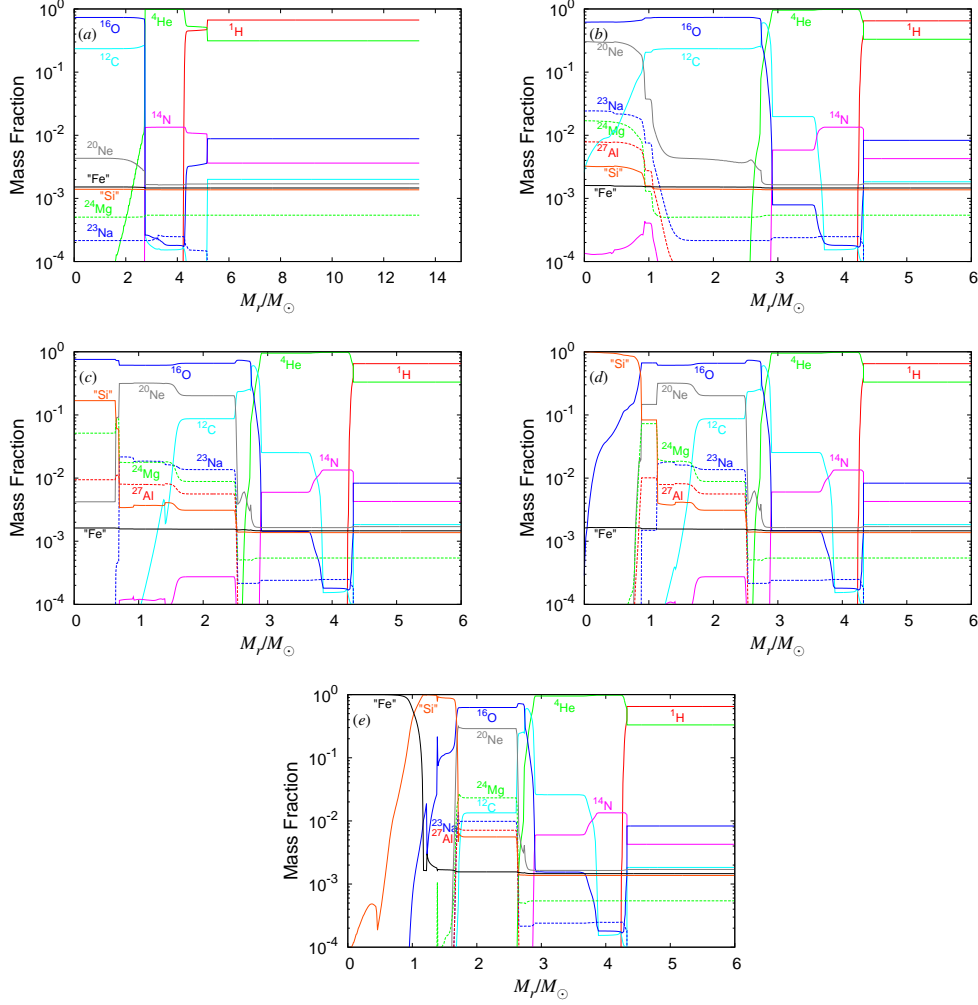


Fig. 2. Mass fraction distributions of a $M = 15M_{\odot}$ star after the He burning (a), C burning (b), Ne burning (c), O burning (d), and Si burning (e). The final mass is $M_f = 13.6M_{\odot}$. “Si” and “Fe” indicate the sum of the mass fractions of the elements Si-Sc and Ti-Br.

core helium burning. There is a CO core of $2.2 M_{\odot}$ in the central region. The He layer of $2 M_{\odot}$ and the H-rich envelope surround the CO core. The He layer consists of ashes of the hydrogen burning. After the core helium burning, the shell helium burning produces ^{12}C in the He layer. Then, the carbon ignites at the center when the central temperature becomes $\log_{10} T_{\text{C}}(\text{K}) \sim 8.8$. The core carbon burning converts ^{12}C into ^{20}Ne and ^{23}Na to form an O/Ne core (Fig. 2(b)). Some Mg-Si are also produced in the core.

The shell carbon burning is followed by the core carbon burning. It converts the O/C layer into an O/Ne layer. However, ^{12}C of 0.09 by mass fraction remains even after shell carbon burning. When the central temperature becomes $\log_{10} T_{\text{C}}(\text{K}) \sim 9.2$, the core neon burning starts and an O/Si core forms (Fig. 2(c)). After the Ne burn-

ing, oxygen ignites at the center with the central temperature of $\log_{10} T_C(\text{K}) \sim 9.3$. The core oxygen burning produces a $\sim 1M_\odot$ Si core (Fig. 2(d)). The main components of the Si core is ^{28}Si , ^{32}S , and ^{34}S and the electron fraction decreases by electron captures. The Si core extends through the following shell oxygen burnings and the central temperature increases by the contraction. When the central temperature is $\log_{10} T_C(\text{K}) \sim 9.55$, the Si burning starts and an Fe core forms (Fig. 2(e)). The composition in the O layer also gradually changes through shell burnings. After the Fe core formation, the Fe core extends with shell Si burning and finally collapses to explode as a supernova.

Here we stress that one of the most important factors in the massive star evolution is the carbon abundance after core helium burning, $X_C(^{12}\text{C})$. In general smaller carbon abundance leads a larger iron core at core collapse. This is because when the carbon abundance is smaller, shell carbon burning is weaker after helium burning. Then the core is less supported by the convective carbon shell burning and the time between the central helium burning to the oxygen burning is shorter. As a result, for smaller carbon abundance a larger core with higher entropy is formed because neutrino cooling is less effective.^{11), 12)}

The carbon abundance also affects on nucleosynthesis substantially. When the abundance is too low, carbon burning products such as Ne, Na, Mg, and Al are underproduced compared with the solar abundance pattern, while they are overproduced when the abundance is too large.³¹⁾ They also found that the abundances of S, Ar, and Ca are anti-correlates with Ne, Na, Mg and Al.

Despite of these importance the carbon abundance is very uncertain because it sensitively depends on the $^{12}\text{C}(\alpha, \gamma)^{16}\text{O}$ rate and the treatment of convection. Ref. 31) discussed that due to the nucleosynthetic constraint described above, in their model the $^{12}\text{C}(\alpha, \gamma)^{16}\text{O}$ rate needs to be 1.7 ± 0.5 times the Caughlan and Fowler (1988) (CF88 hereafter) rate.³²⁾ In the NH88 model¹²⁾ the rate of Ref. 33) was taken which corresponds to 2.3 – 2.4 times the CF88 rate. In NH88, $X_C(^{12}\text{C}) = (0.25, 0.22, 0.19)$ for the helium star model for $M_{\text{He}} = (3.3, 6, 8) M_\odot$, which roughly corresponds to the ZAMS $M = (13, 20, 25) M_\odot$, respectively. In the UN model the $^{12}\text{C}(\alpha, \gamma)^{16}\text{O}$ rate was chosen to be 1.3 times larger than the CF88 rate so that the abundance pattern of EMP and VMP stars are reproduced.^{22), 34)}

Although there have been improvements in the estimation of the $^{12}\text{C}(\alpha, \gamma)^{16}\text{O}$ rate^{35), 36)} uncertainty in the rate is still about factor of two. Therefore, the nucleosynthetic method is still the best way to constrain the carbon abundance.

We show in Table I the central carbon abundance after the core helium burning for UN and YU models. In the YU model $^{12}\text{C}(\alpha, \gamma)^{16}\text{O}$ rate is chosen to be 1.5 times as large as the CF88 rate so that the carbon abundance $X_C(^{12}\text{C}) = 0.20$ for the $M = 25M_\odot$ model. As shown in the table, mainly because of the difference in the $^{12}\text{C}(\alpha, \gamma)^{16}\text{O}$ rate, the YU models presented in this paper have systematically smaller carbon abundance than the UN models. In Table II we show also final, M_f , He core, M_{He} , and CO core masses, M_{CO} . Here the latter two masses are defined where the mass fraction of H and He are less than 0.001, respectively.

Table I. Carbon mass fraction after core He burning for UN and YU models.

UN model							
$M(M_\odot)$	11.5	12	13	15	20	22	25
$X_C(^{12}\text{C})$	0.36	0.36	0.33	0.36	0.34	0.28	0.26
YU model							
$M(M_\odot)$	11	12	13	15	18	20	25
$X_C(^{12}\text{C})$	0.26	0.25	0.31	0.24	0.23	0.23	0.20

Table II. Final, core and remnant masses for UN, YU and NH88 models.

UN model							
$M(M_\odot)$	11.5	12	13	15	20	22	25
$M_f(M_\odot)$	11.2	11.6	12.7	13.9	17.5	17.6	17.7
$M_{\text{He}}(M_\odot)$	2.8	3.0	3.3	4.0	5.3	6.7	7.9
$M_{\text{CO}}(M_\odot)$	1.62	1.72	1.95	2.51	3.91	5.42	6.54
$M_{\text{rem}}(M_\odot)$	1.40	1.43	1.45	1.51	1.57	1.66	1.70
$M_g(M_\odot)$	1.26	1.29	1.30	1.35	1.40	1.46	1.50
YU model							
$M(M_\odot)$	10	11	12	13	15	18	20
$M_f(M_\odot)$	9.5	10.5	11.4	12.1	13.6	16.2	17.6
$M_{\text{He}}(M_\odot)$	2.6	2.8	3.1	3.2	4.2	5.4	6.2
$M_{\text{CO}}(M_\odot)$	1.47	1.61	1.81	1.87	2.64	3.58	4.34
$M_{\text{rem}}(M_\odot)$	1.29	1.32	1.44	1.45	1.64	1.77	1.96
$M_g(M_\odot)$	1.18	1.19	1.29	1.30	1.45	1.55	1.69
NH88 model							
$M(M_\odot)$	~ 13	~ 15	~ 20	~ 25			
$M_{\text{He}}(M_\odot)$	3.3	4	6	8			
$M_{\text{rem}}(M_\odot)$	1.27	1.33	1.61	1.77			
$M_g(M_\odot)$	1.15	1.20	1.43	1.55			

3.1. Evolution of 10-13 M_\odot stars

Here we describe the evolution of 10-13 M_\odot stars calculated by the YU code since these stars correspond roughly to the lightest Fe core collapse model, and the evolution after oxygen burning is quite different from more massive $M > 13M_\odot$ stars. Table III shows the differences in the way how the stars commence nuclear burning of Ne, O, and Si. In the table a letter ‘C’ represents that the ignition occurs at the center of the core and ‘off-C’ shows that the ignition occurs off-centrally. In the line of the composition, letters represent main nuclei at the center. The differences also appear in Fig. 3, in which evolutionary tracks are shown in terms of the central temperature and density. In this mass range, a star forms a CO core around the Chandrasekhar limiting mass. The degeneracy of the core is the important property and affects its evolution.

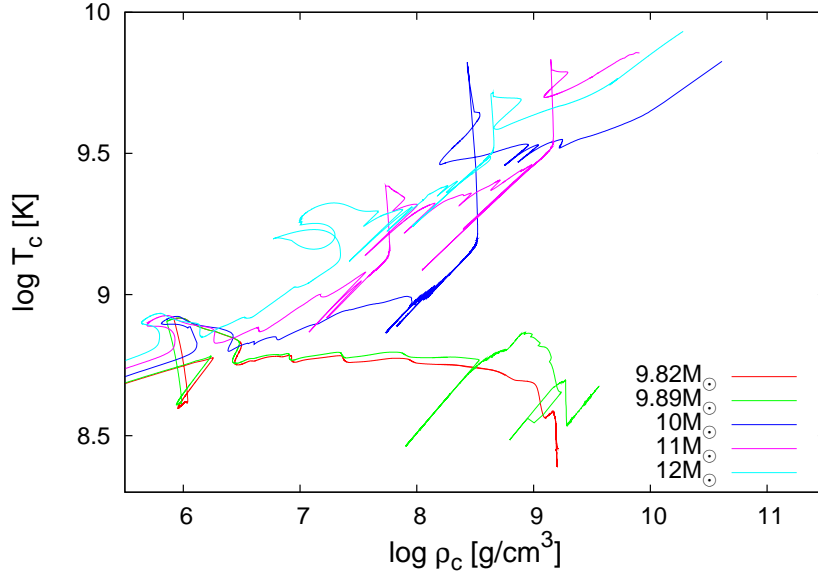


Fig. 3. Evolution tracks of $M = 9.82, 9.89, 10, 11$, and $12M_{\odot}$ stars in terms of central temperature and density.

We will present more detailed description in Takahashi, Yoshida & Umeda (2012, in preparation, see also Ref. 37)), in which stellar evolutions are calculated in very fine grids. So far, we have found that $M = 9.89M_{\odot}$ model ends up the Fe core formation, though $M = 9.82M_{\odot}$ model does not form an Fe core. As described below the off-center Si-burning is more and more violent for less massive stars. In this mass range only $0.01 M_{\odot}$ difference in the zero-age main sequence mass would result in quite different evolution. However, the global evolutionary properties and final density structure of an Fe core is similar to the $10 M_{\odot}$ model presented here as far as an Fe core is formed.

10 M_{\odot} star: For a $10 M_{\odot}$ star, the evolution from the zero age main sequence to the C burning phase goes roughly in the same way as more massive stars which end up with the Fe core formation. However, after an O-Ne core formation through the C burning, different evolutionary aspects come about.

Because the mass of the C-O core of $1.47M_{\odot}$ is only slightly larger than the critical mass for the Ne ignition, the O-Ne core first contracts without nuclear burning. Eventually, the importance of the pressure of degenerate electron increases. Such semi-degenerate cores often show the inverse temperature distribution; temperature does not take its highest value at the center. This is due to the property of degenerate electrons. Since neutrino cooling is more effective at higher density as well as at higher temperature, the O-Ne core loses its heat by the cooling. As heat escapes, the core contracts and compressional heating supply energy into the gas of ions, electrons, and radiation. If the core is supported by pressure of ions, gas temperature increase as a result of compressional heating. On the other hand, if electron pressure supports the core, gas temperature is hard to increase because internal en-

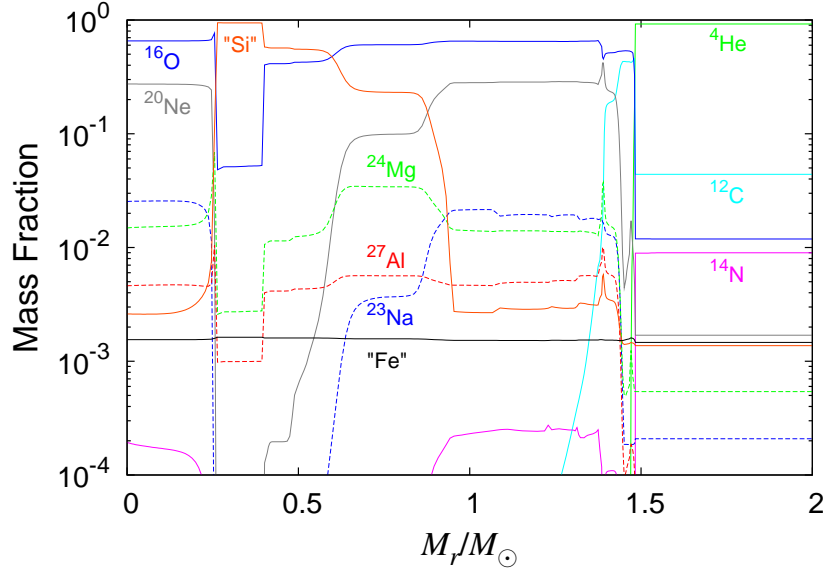


Fig. 4. Mass fraction distribution for a $10M_{\odot}$ star during a shell Ne+O burning, when $\log_{10} \rho_C = 7.9358$.

ergy of degenerate electrons does not depend on temperature but on density. What the high density O-Ne core supports mainly is the pressure of degenerate electrons, so the denser the region is, the slower the temperature increase is. Owing to this temperature inversion, a shell Ne burning commences at an off-center region having higher temperature than the center. Since Ne and O have close ignition temperatures, once the shell Ne burning commences, heat generation increases temperature and the shell O-ignition succeeds. Then a degenerate O-Ne core is surrounded by a hot Si-shell (Fig.4). These evolutionary properties are fully consistent with previous works (e.g., Refs. 12), 8)).

Some of the nuclei of the Si cluster produced by the O burning can capture electrons in such a high density O-Ne core. Since the core is mainly supported by the pressure of degenerate electrons, the decrease of the number of electrons causes the core contraction. Heat production by the contraction increases the temperature. When temperature at the base of the Si shell becomes high enough to ignite Si, the shell Si burning commences and transforms the Si shell into the Fe shell (Fig. 5). The energy production rate of the burning from Ne to Fe is very high. So at every ignition, the core repeats the expansional cooling and compressional heating almost adiabatically,^{*)} and the burning front approaches the center little by little. After the burning front reaches the center of the core, an Fe core forms. Then the star collapse. Some vertical ascents in Fig. 3 show moments when a base of a off-center burning reaches the center of the core. For a $10M_{\odot}$ star, the central temperature suddenly increase at $\log_{10} \rho_C = 8.4319$ when the shell Ne+O+Si burning reaches the center.

^{*)} This is seen in spikes around $\log_{10} \rho_C \sim 8$ in Fig. 3.

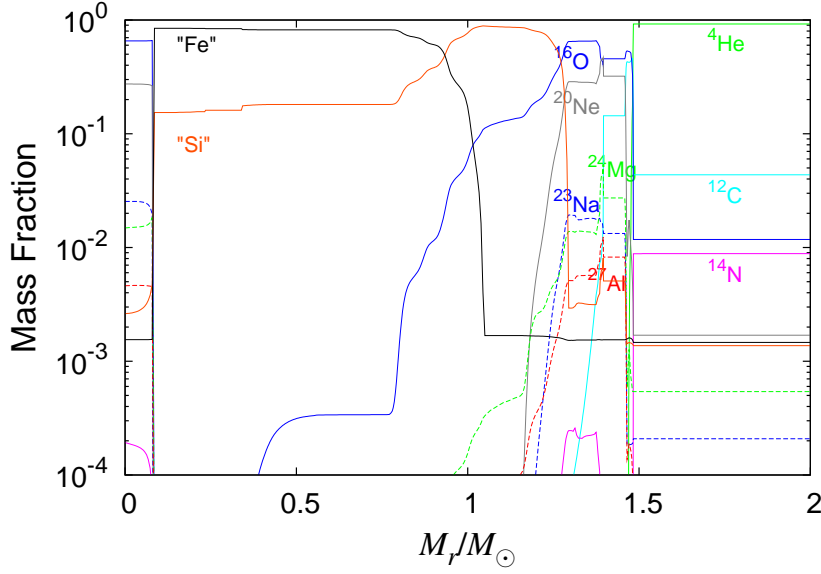


Fig. 5. Mass fraction distribution for a $10M_{\odot}$ star during a shell Ne+O+Si burning, when $\log_{10} \rho_C = 8.0958$.

11 M_{\odot} star: For a 11 M_{\odot} star with a larger C-O core of $1.61M_{\odot}$ than a $10M_{\odot}$ star, electron degeneracy of the core is less. This causes the difference in evolution after Ne and O ignite off-centrally.

Because of the less degeneracy at the center, a difference between the maximum and the central temperature is less, so a shell O+Ne ignition commences at deeper region than the $10M_{\odot}$ star (Fig. 6). The temperature at the base of the shell increases by compressional heating as the same way as the $10M_{\odot}$ star during the O+Ne burning front propagation. However, the burning front arrives at the center before the base temperature reaches the Si ignition and, thus, a Si core forms. This is the main difference between 10 and $11M_{\odot}$ stars.

Later, as the Si core contracts, outer O+Ne shell burning repeats moving its base outward, while neutron rich nuclei such as ^{36}S and ^{50}Ti are produced in inner region. Degeneracy of electrons also increases in the contracting core and the above-mentioned temperature inversion appears. When the central density reaches the value of $\log_{10} \rho_C = 8.9867$, the first off-center Si ignition occurs at $M_r = 0.5933M_{\odot}$. This ignition causes the core to expand adiabatically. After the burning terminates, the core contracts adiabatically again. When the central density becomes $\log_{10} \rho_C = 9.0253$, the second off-center Si ignition occurs at $M_r = 0.1103M_{\odot}$ (Fig. 7). After the second off-center Si ignition, the burning front reaches the center. The core transforms into an Fe core, then collapses.

12 M_{\odot} star: A $12M_{\odot}$ star evolves similar to a $11M_{\odot}$ star but the properties of Ne and O ignitions are different. Because it has a larger C-O core of $1.85M_{\odot}$, temperature takes its highest value at the center of the O-Ne core. Therefore, Ne and O ignite at center. Note that Table III shows that when O ignites at the center,

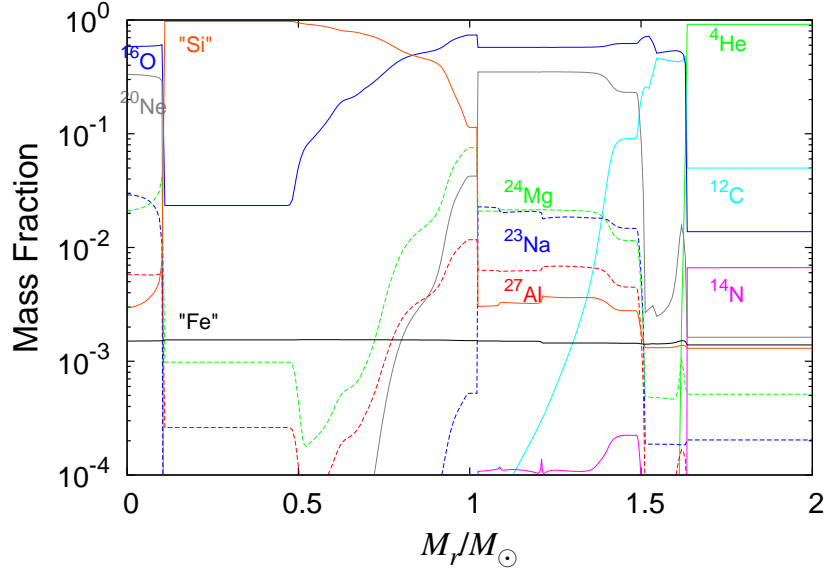


Fig. 6. Mass fraction distribution for a $11M_{\odot}$ star during a shell Ne+O burning, when $\log_{10} \rho_C = 7.6181$.

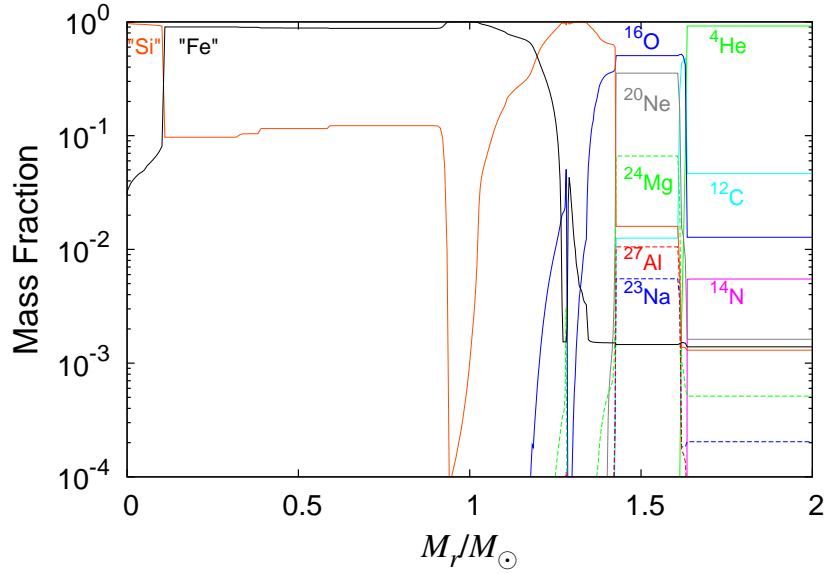


Fig. 7. Mass fraction distribution for a $11M_{\odot}$ star during a shell Si burning, when $\log_{10} \rho_C = 8.0481$.

central composition is O-Si, and not O-Ne. This is just because Ne has burned ahead of O, producing a O-Si core.

After Si core formation, the evolution proceeds as the same way as a $11M_{\odot}$ star. Neutron rich nuclei are produced around the center after several shell Ne+O burning at outer regions of the contracting core. Then off-center Si burning occurs (Fig. 8),

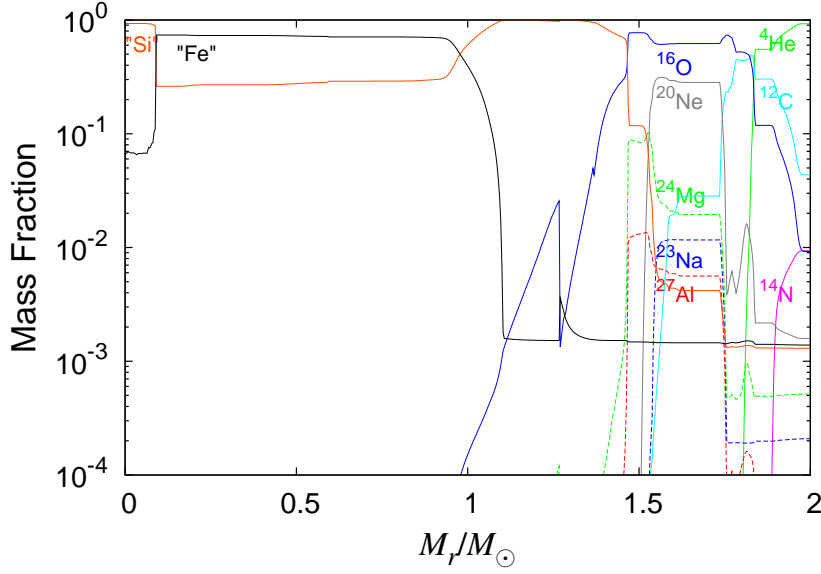


Fig. 8. Mass fraction distribution for a $12M_{\odot}$ star during a shell Si burning, when $\log_{10} \rho_C = 7.9694$.

and after the front reaches the center an Fe core forms.

Table III. Ignition properties of $10 - 13M_{\odot}$ stars.

C ignition	$10M_{\odot}$	$11M_{\odot}$	$12M_{\odot}$	$13M_{\odot}$
at the center or not	C	C	C	C
central composition	C-O	C-O	C-O	C-O
Ne ignition	$10M_{\odot}$	$11M_{\odot}$	$12M_{\odot}$	$13M_{\odot}$
at the center or not	off-C	off-C	C	C
central composition	O-Ne	O-Ne	O-Ne	O-Ne
O ignition	$10M_{\odot}$	$11M_{\odot}$	$12M_{\odot}$	$13M_{\odot}$
at the center or not	off-C	off-C	C	C
central composition	O-Ne	O-Ne	O-Si	O-Si
Si ignition	$10M_{\odot}$	$11M_{\odot}$	$12M_{\odot}$	$13M_{\odot}$
at the center or not	off-C	off-C	off-C	off-C
central composition	O-Ne	Fe-Si	Fe-Si	Fe-Si

3.2. Final mass and metallicity

In Fig. 9 we show the metallicity dependence of the final and core masses of the YU models.²⁰⁾ We see clear metallicity dependence in the final mass among the stars with $M \gtrsim 20M_{\odot}$. In $Z = 0.02$, $M = 30M_{\odot}$ star has the maximum final mass: $M_f = 21.3M_{\odot}$. $M \gtrsim 40M_{\odot}$ stars indicate a roughly constant final mass of $\sim 10M_{\odot}$. These stars lose all of H and He layers and become Wolf-Rayet stars. Effect of mass loss in $Z = 0.01$ stars is less than that in $Z = 0.02$ stars. Increasing the main-

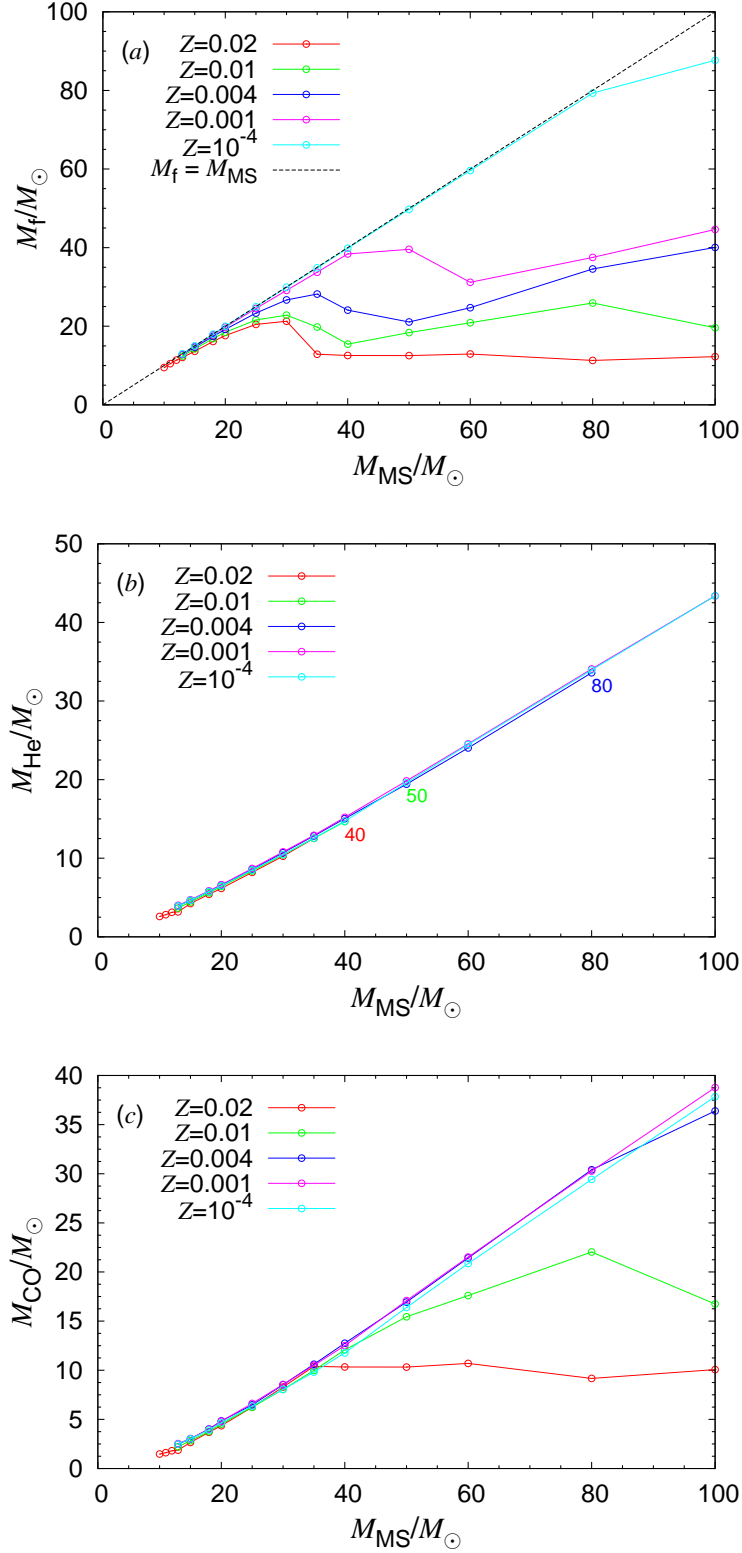


Fig. 9. The final mass (panel (a)), the He core mass (panel (b)), and the CO core mass (panel (c)) with the relation to the main-sequence mass. The adopted metallicities are $Z = 10^{-4}$, 0.001, 0.004, 0.01, and 0.02. In panel (b), stars more massive than the attached number of the main-sequence mass (M_{\odot}) evolve to WO stars. The surface He mass fraction of the stars is about 0.2.

sequence mass, the final mass also increases in $M \leq 30M_{\odot}$ and $40 \leq M \leq 80M_{\odot}$ but it decreases in $30 \leq M \leq 40M_{\odot}$ and $M \geq 80M_{\odot}$. Metal poorer stars have similar M dependence of the final mass. In this figure the zero-age main-sequence mass where the mass loss becomes effective and the final mass for a given main-sequence mass become larger for metal poorer stars. We do not see clear mass loss effect among $M \leq 80M_{\odot}$ stars with $Z = 10^{-4}$.

The metallicity dependence of the He core is small (Fig. 9(b)). On the other hand, most of the He layer has lost during the evolution in $M \geq 40, 50$, and $100 M_{\odot}$ stars for $Z = 0.02, 0.01$, and 0.004 . These stars lose the He/C/O envelope and their surface He abundance decreases during the He burning. They become C- and O-enriched Wolf-Rayet stars (WO stars) with the surface He mass fraction of ~ 0.2 . The mass of the He-rich shell is $1.4 - 5.5M_{\odot}$ in $Z = 10^{-4}$ stars, in which mass loss effect is small. Since the fraction of the He layer is small, mass loss brings about the removal of He layer rather than the reduction of the He core mass.

The metallicity dependence of the CO core mass is seen in $Z > 0.004$ and $M \gtrsim 40 - 50M_{\odot}$ in Fig. 9(c). The CO core mass is roughly constant with $\sim 10M_{\odot}$ in $Z = 0.02$ and $M \geq 40M_{\odot}$ stars. In $Z = 0.01$, the maximum mass of the CO core is $22M_{\odot}$ of $M = 80M_{\odot}$ star. On the other hand, the CO core mass can be more massive in metal-poorer stars. The CO core mass is $35 - 40M_{\odot}$ in $Z \leq 0.004$ and $M = 100M_{\odot}$.

§4. Nucleosynthesis

Nucleosynthesis in these massive stars occurs mainly in two stages. One is before core-collapse and the other is during supernova explosion. It is well known that inside these massive stars nuclear fusion takes place up to Fe synthesis. Before gravitational core collapse, Fe core is produced at center and lighter elements form onion like structures from inside to the surface (Fig. 10).

Nucleosynthesis during the supernova explosion is usually called *explosive nucleosynthesis*. During the explosion, shock wave propagates out of Fe-core to the stellar surface. Behind the shock wave matter heats up and nuclear burning takes place. Explosive nucleosynthesis is important for the synthesis of Si and heavier elements (e.g., Ref. 16)).

In our previous works (e.g., Refs. 16), 22), 17), 38)) we use a simple 1D model for supernova explosion to calculate explosive nucleosynthesis. We inject thermal or kinetic energy below the mass cut or just above the Fe core to initiate supernova shock. We may call this procedure as 'instant energy injection'.

We use a 1D PPM code for the hydrodynamical calculations and solve small alpha-network together to calculate nuclear energy generation. Then we calculate detailed nucleosynthesis post-processingly by solving a large nuclear reaction network.

Explosive nucleosynthesis should depend on how the star explodes, but we do not know yet how gravitational collapse leads to the explosion. Therefore, there are still several proposals for the successful supernova explosions. Fortunately the properties of supernova shock outside the Fe core is almost independent of the explosion

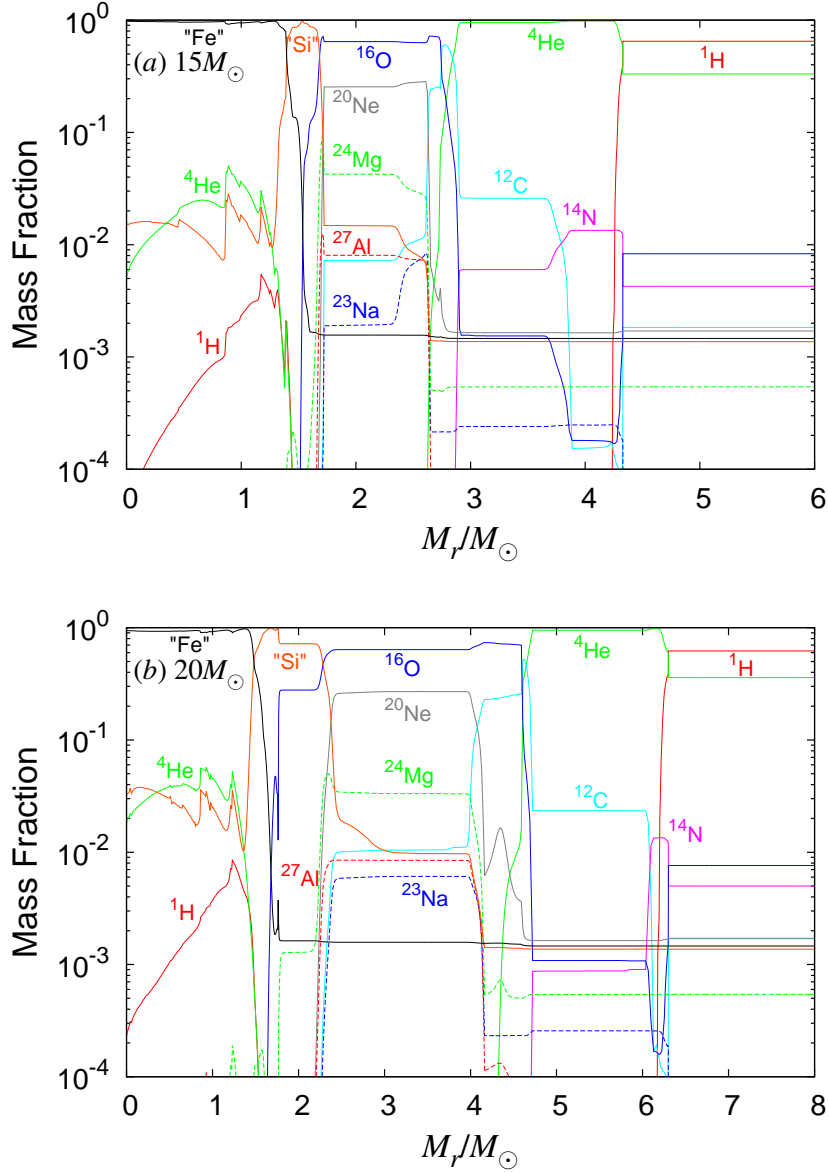


Fig. 10. Mass fraction distribution of the supernova progenitors evolved from 15 (a) and 20 M_\odot (b) stars with the metallicity of $Z = 0.02$. The corresponding final masses are 13.6 and 17.6 M_\odot . The mass fraction distribution in the H-rich envelope outside the range of each figure is the same as that at the outer edge of the figure.

mechanism, because in most models the supernova shock gains energy inside the Fe core. Then, as far as spherical symmetry is assumed, explosion energy E is the only parameter which determines the properties of the supernova shock. For example, kinetic to thermal energy ratio does not much affect the propagation of the shock outside the Fe core, because it quickly converges into the same solution. In this case

'instant energy injection' method is sufficient to calculate nucleosynthesis. For most cases, nucleosynthesis of Fe peak elements including Zn and lighter elements can be safely calculated with this method. In Section 7, We will discuss the limitations of this simple procedure.

Behind the shock front, temperature distribution is almost homogeneous, and the radiation energy is strongly dominated. Then the radiation temperature T can be related to the explosion energy, E , by $E = (4\pi/3)ar^3T^4$, where a is the radiation constant and r is the shock radius. Thus the maximum temperature after shock passage, T_s , for the mass elements located at radius R in the progenitor is approximately given as³⁹⁾

$$T_s = (3E/4\pi aR^3)^{1/4}. \quad (4.1)$$

For a given progenitor model and explosion energy E , the propagation of shock and thus the time evolution of density distribution is also determined uniquely. Behind the shock front, pressure and entropy are also radiation dominated and can be written as $P_\gamma = aT^4/3$ and $S_\gamma = (4/3)aT^3/\rho$. Since the shocked region cools roughly adiabatically at first, the radiation entropy is often convenient to specify the explosion.

In the inner most region of supernova ejecta where T_s is higher than 5×10^9 (K), Si burns completely. In such a region, at first Si mostly decomposes to alpha-particles, and this is endothermic reaction. Then as the temperature decreases alpha particle starts to recombine and alpha-rich freezeout nucleosynthesis takes place. This phase is exothermic. The energy changes due to these processes are typically about ten percent, and thus above equation (4.1) still provides a useful approximation.

In this 'complete Si burning' region ^{56}Ni is dominantly produced but also Co, Ni, and Zn are mostly produced here. The final abundance depends on entropy because the mass fraction of alpha-particles during the alpha-rich freezeout phase increases with entropy.³⁹⁾

For example, one of the authors has shown that high entropy during the hypernova explosion explains well the larger ratio of $[\text{Zn}/\text{Fe}]$ and $[\text{Co}/\text{Fe}]$ towards lower metallicity, $[\text{Fe}/\text{H}]$, in extremely metal poor (EMP) stars.^{16), 22), 34), 40)} They also discussed that simple 1D model cannot explain the abundance of EMP stars by the hypernova models, because Fe or ^{56}Ni is over-ejected to satisfy the large $[\text{Zn}/\text{Fe}]$ ratio. This problem and the solution is described in the subsection 4.3.

When T_s is between $4 - 5 \times 10^9$ (K), Si burns incompletely. This region is called incomplete Si burning region. Main products here is Cr, Mn, and ^{56}Ni . For $T_s \simeq 3 - 4 \times 10^9$ (K), oxygen burns partially and Si, S, Ar, Ca, Ti, V are main products. In these regions also nuclear burning produces some amount of energy. In summary, previous works have shown that explosive nucleosynthesis up to Zn can be described well by instant energy injection models, though hypernova models over-produce Fe in simple spherically symmetric models.

So far we have not mentioned the effects of neutrino process (ν -process), but the process is important for some elements such as Li, B, F, and Mn.^{41), 42), 43), 44), 45), 38), 46), 47), 48), 49), 50)} Of course the neutrino emission depends on the explosion model and thus we have to

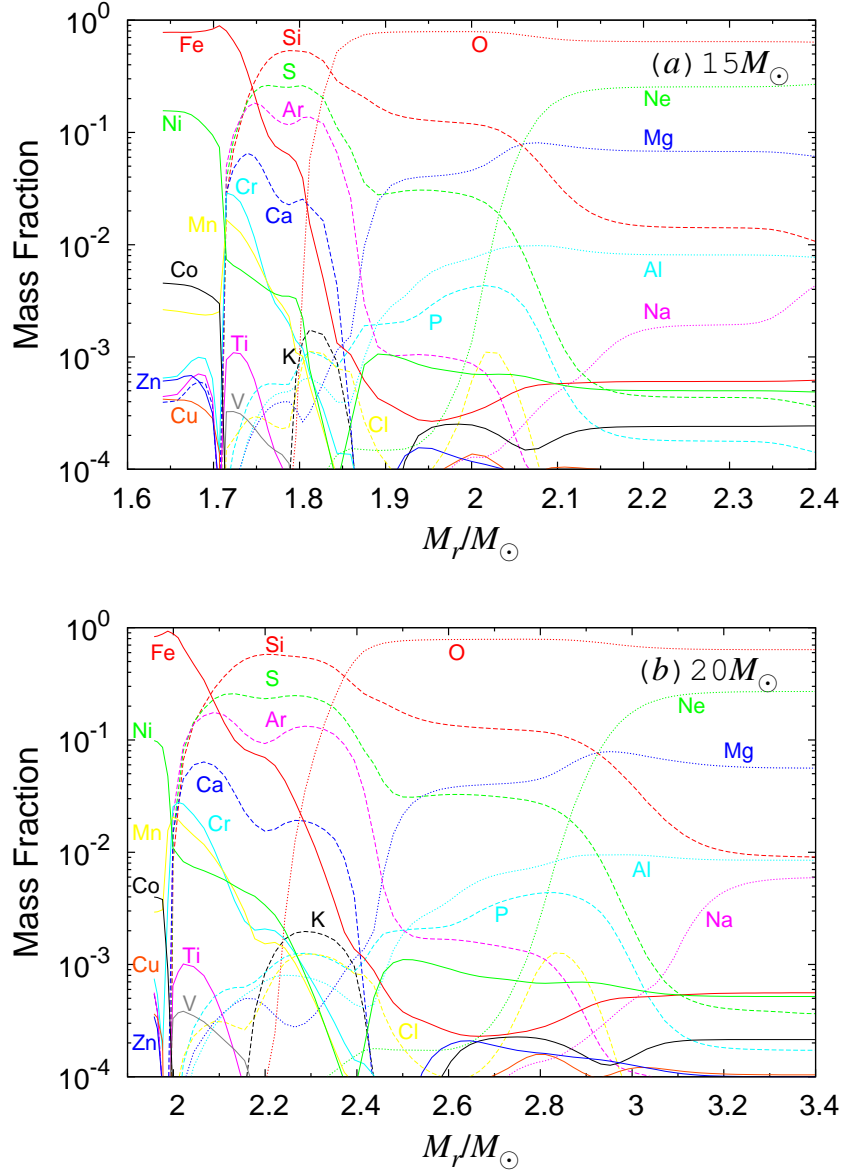


Fig. 11. Mass fraction distribution of the innermost region of the supernova ejecta evolved from from 15 (a) and $20 M_\odot$ (b) stars with the metallicity of $Z = 0.02$. The explosion energy is set to be 1×10^{51} erg.

assume a model to include the effects (see Ref. 38) for the detail). Fig. 12 shows the mass fraction distributions of Li, B, F, Sc, V, and Mn of the supernova ejecta evolved from a $15 M_\odot$ star with $Z = 0.02$. In this calculation, we assume that the neutrino luminosity decreases exponentially with the decay time of 3 s. The total neutrino energy is set to be 3×10^{53} erg. The neutrino spectra are assumed to obey Fermi distribution with zero chemical potential. The temperatures of $\nu_{\mu,\tau}$, $\bar{\nu}_{\mu,\tau}$ and ν_e , $\bar{\nu}_e$

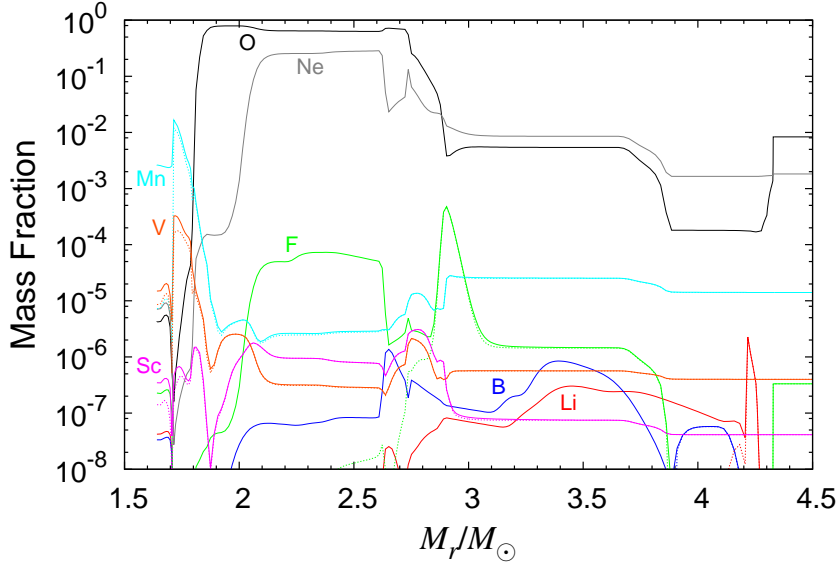


Fig. 12. Mass fraction distribution of Li, B, F, Sc, V, and Mn produced through the ν -process in the supernova ejecta evolved from a $15 M_{\odot}$ star with the metallicity of $Z = 0.02$. Solid and dotted lines indicate the mass fractions of the elements with and without the ν -process, respectively.

are set to be 6 MeV/ k and 4 MeV/ k , respectively, as in Ref. 38). Almost all Li and B are produced through the ν -process in the O/Ne-layer and He-layer. When the ν -process is not taken into account, the mass fractions of Li and B are smaller than the lowest value in this figure. Large F production through the ν -process is obtained in the O/Ne layer (see also Refs. 49), 50)). A part of F is produced in the explosive He burning from ^{15}N . Although the F production from ^{15}N strongly depends on the metallicity, the F production through the ν -process scarcely depends on the metallicity and, thus, it is important throughout the Galactic chemical evolution. Parts of Sc, V, and Mn are produced through the ν -process, especially in the complete and incomplete Si-burning regions.

4.1. $X_{\text{C}}(^{12}\text{C})$ and abundance pattern of Ne to Ca

In the previous section, we mentioned that the carbon abundance after helium burning is important for the abundance of Ne to Ca. Here we look the results of UN and YU models more closely. In Fig. 13 we show $[X_i/\text{O}]$ vs. atomic number. Here X_i represents Salpeter's initial mass function (IMF) weighted yields of Ne to Ca isotopes, and $[A/B] = \log_{10}(Y_A/Y_B) - \log_{10}(Y_A/Y_B)_{\odot}$, where Y_A and Y_B are the abundances of elements A and B. If any point is far from the solar value, $[X_i/\text{O}] = 0$, the model fails to explain the present day abundance, though chemical evolution model should be applied for a detailed discussion. This figure shows that for both models, each point is roughly in the ± 0.3 range, thus these models would yield roughly solar abundance pattern.

Since UN model has larger $X_{\text{C}}(^{12}\text{C})$ after helium burning, this model has larger

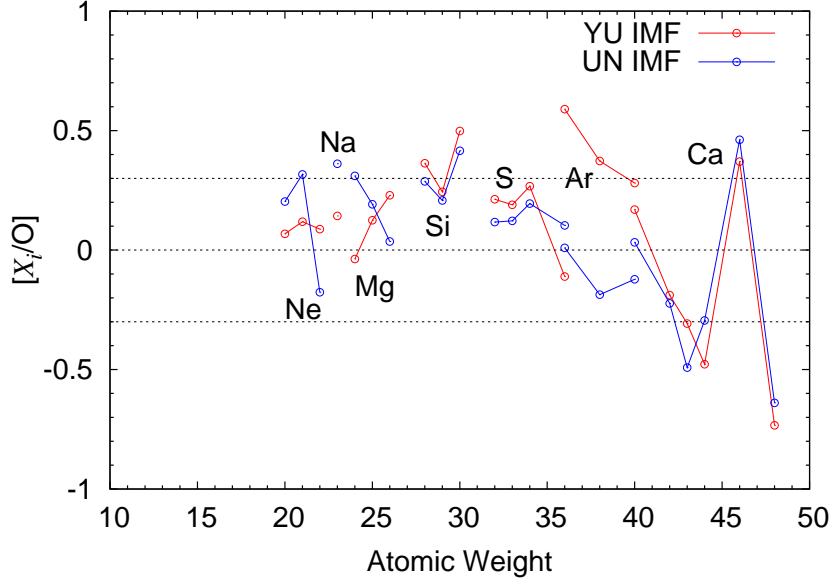


Fig. 13. The IMF weighted yield ratios $[X_i/O]$ as a function of atomic weight. Red and blue lines indicate the yield ratios in YU model and UN model, respectively.

Ne/O and Na/O ratios than the YU model as expected. Larger $X_C(^{12}\text{C})$ means that smaller $X_C(^{16}\text{O})$ and thus explosive oxygen burning products, such as S, Ar, Ca, would be less abundant. This is also seen in the figure.

The UN yields calculated with the same parameter choices was applied to the Galactic chemical evolution model in Ref. 51). It was shown that the model could reproduce the observed abundance pattern reasonably well. If we look the results closely, however, $[\text{Na}/\text{Fe}]$ is slightly larger than zero at $[\text{Fe}/\text{H}]=0$, and $[\text{Ca}/\text{Fe}]$ and $[\text{Ar}/\text{Fe}]$ are slightly smaller than zero at $[\text{Fe}/\text{H}]=0$. This suggests that slightly larger $^{12}\text{C}(\alpha, \gamma)^{16}\text{O}$ rate may reproduce the solar abundance better at $[\text{Fe}/\text{H}]=0$. Using the YU codes we will investigate the best choice of the $^{12}\text{C}(\alpha, \gamma)^{16}\text{O}$ rate, or the $X_C(^{12}\text{C})$, in a forthcoming paper.

4.2. Zn abundance in EMP stars and asphericity of hypernovae

Observations of extremely metal poor (EMP) stars, which are defined as halo stars with $[\text{Fe}/\text{H}] < -4$, revealed that $[\text{Zn}/\text{Fe}]$ and $[\text{Co}/\text{Fe}]$ are larger than higher metallicity stars (e.g., Ref. 52)). Ref. 16) proposed that these large ratios are explained by the ejecta of complete Si burning of hypernova. This idea explains also why such EMP stars have low $[\text{Fe}/\text{H}]$. In the early universe where the metal abundance in inter stellar matter (ISM) was low, the Fe to H ratio was determined by the amount of Fe produced by a supernova over that of hydrogen swept by the supernova shock. Since the swept hydrogen mass is roughly proportional to the explosion energy, the ejecta of a hypernova tends to have lower $[\text{Fe}/\text{H}]$ than that of a supernova.

As mentioned above, however, there is one problem for this idea. Zn and Co are produced mainly in the complete Si burning while Fe or ^{56}Ni is produced both in

complete and incomplete Si burning regions. Therefore, $[\text{Zn}, \text{Co/Fe}]$ becomes larger when relatively more material is ejected from the complete Si-burning region. Under the assumption of spherical symmetric explosion, this means that the mass-cut has to be taken sufficiently deep, then the ejected mass of Fe or ^{56}Ni also increases. On the other hand if too much Fe is ejected O/Fe ratio, for example, becomes too small compared with observations. To quantify this problem Ref. 16) introduced the 'mixing-fallback model'. In the model, yields are calculated as follow. First, inner most matter is mixed between the mass coordinate M_{in} and M_{out} . For hypernova models M_{out} is set to the upper boundary of the incomplete Si burning region, and M_{in} is chosen sufficiently deep to eject Zn. Then it is assumed that only the fraction f of the matter is ejected, or the fraction $1 - f$ fallbacks, from this region. To explain the abundance pattern of EMP stars $f \sim 0.1$ is required.

For supernova models with $M < 25M_{\odot}$, $f=1$ is fine to reproduce abundance pattern of very metal poor stars with $-3 < [\text{Fe/H}] < -2$.³⁴⁾ This suggests that the explosion mechanism of supernova and hypernova is different.

Interestingly almost the same yield as the $f \sim 0.1$ hypernova yield could be obtained when we calculate jet-like hypernova models in 2D.⁵³⁾ In such models, it is assumed that an unknown central engine ejects jets along the polar directions. These jets can blow up the entire star above the Si layer, but the explosive Si burning mainly takes place along the jet directions. As a result the mass fraction of complete Si burning products becomes smaller than the spherically symmetric models. In this paper also in §6.3 we show such a 2D calculations applied to an initially $M = 110M_{\odot}$ star. Since observed hypernovae show some asphericity,⁵⁴⁾ this jet-like explosion model is certainly interesting, though we need to know the mechanism for the central engine.

It is sometimes claimed that Zn and Co in EMP stars may be explained by the innermost matter from 'hot bubble' region of normal supernovae (e.g., Ref. 55)). Ref. 56) explored this possibility and discussed that this explanation is not likely because fine tuning of $Y_e (= 0.500 - 0.501)$ is required for a $0.06 M_{\odot}$ ejecta to produce sufficient amount of Zn and Co. These conditions are difficult to satisfy for the hot bubble matter of supernovae, while it is relatively easy for the innermost ejecta of hypernovae.

4.3. Nucleosynthesis of (weak) r-process elements

It is quite likely that during explosion supernovae produce elements heavier than Zn, because some EMP stars have r- and weak-r process elements. For example CS22892-052 shows r-process abundance pattern which is roughly same as the present-day r-process pattern.⁵⁷⁾ This suggests that the r-process nucleosynthesis is almost *universal*. There are other classes of stars which show more abundance of weak r-process elements such as Sr, Y, Zr than the universal r-process pattern. There are also some stars having enhancement of Mo and Ru as well as Sr, Y, Zr stars.⁵⁸⁾

As mentioned above spherically symmetric instant energy injection models cannot synthesize such elements because to synthesize such elements much larger entropy and/or more neutron rich environment are required. On the other hand Fe-peak ele-

ments including Zn can be synthesized from the matter with $Y_e \simeq 0.50$. Most recent 1D core collapse supernovae simulations have shown that the innermost matters in the ejecta have $Y_e \simeq 0.50$ or even greater than 0.5 because of the interaction with neutrinos (e.g., Refs. 59,60,61)).

Ref. 40) and 56) explored the conditions for synthesizing weak r-process elements, Sr, Y, and Zr. Typically innermost layers of normal supernova explosions have entropy per baryon $s/k \sim 5$ and those of hypernovae have $s/k \sim 15$. With such entropy weak r-process elements are not produced if $Y_e \simeq 0.50$. Thus they relaxed the constraint $Y_e \simeq 0.50$ and considered Y_e as low as 0.45. Such low Y_e matter cannot be ejected as long as we consider exact spherically symmetric explosion. However, as shown in Ref.62) in 2D calculations inner materials are mixed by convection during explosion and small amount of low $Y_e \sim 0.45$ and higher entropy $s/k \sim 40 - 50$ matter, may be ejected. Ref. 40) showed that $s/k \gtrsim 15$ model could produce Sr, Y, Zr explosively. Therefore, such low Y_e matter ejected due to the multi-dimensional effects can explain the origin of weak r-process elements.

We note that $s/k \lesssim 50$ models could produce up to Zr but not heavier elements. Because of the lack of observations it is not clear yet weak r- stars which have enhancement of Sr, Y, Zr always have Nb-Mo enhancements as well. If this is the case, innermost matter of hypernovae or hot bubble of normal supernovae considered in Ref. 40) may not be the main site for the weak r-process synthesis. To produce Nb-Mo much larger entropy ($s/k \sim 150$) is required.⁵⁶⁾ It is currently not clear which astronomical site has such an environment.

§5. Remnant neutron star mass

In this section we present remnant neutron star mass in both the UN and YU models and discuss their implications. There are several factors to determine the mass such as the CO-core mass, explosion energy and EOS. Among them the most important factor is the CO-core mass, which is determined by the stellar evolution before core-collapse. Larger CO-core leads larger remnant mass because it typically leads larger Fe-core and, more importantly it increases the amount of mass above the Fe-core.

Once pre-explosion density structure is given, explosion energy determines the mass-cut or remnant neutron star mass M_{rem} . For a given progenitor model, larger explosion energy blows up more materials above the Fe-core leading smaller mass-cut. In this paper, however, as well as our previous works, we do not determine mass-cut in this dynamical way but determine it by the amount of the ejected ^{56}Ni amount, $M(^{56}\text{Ni})$. This is because $M(^{56}\text{Ni})$ is rather sensitive to explosion energy when we determine the mass-cut dynamically. In reality each SN may eject somewhat different amount of ^{56}Ni . However, when we apply the supernova yields for example to the Galactic chemical evolution it is more useful to provide averaged yields. For this purpose it is better to determine the mass-cut by $M(^{56}\text{Ni})$.

We set the explosion energy as $E_{\text{exp}} = 10^{51}$ erg, and the ejected ^{56}Ni amount as $0.07 M_{\odot}$ to determine M_{rem} . $M(^{56}\text{Ni})=0.07 M_{\odot}$ is the value for the SN1987A⁶³⁾ and considered typical value for normal core-collapse SNe. Strictly speaking to eject the

same amount of ^{56}Ni more massive core requires larger E_{exp} . However, the resultant M_{rem} is not much different, so we fix the E_{exp} for simplicity.

In Table II, we show the baryon mass of the remnant neutron star mass by M_{rem} . It correlates with the CO-core mass, which in turn correlates with the He-core mass. The UN model leaves smaller remnant than the YU model for the same initial mass, M , mainly because $X_{\text{C}}(^{12}\text{C})$ after He-burning is larger and thus M_{CO} is smaller as described in §3.

As described, the choice $M(^{56}\text{Ni})=0.07 M_{\odot}$ is a typical value, but this is of course not the unique value (see e.g., a review in Ref. 64)) Therefore, we should remind this fact when we compare with observations. For example, when $M(^{56}\text{Ni})=0.01 M_{\odot}$ in the YU model, $M_{\text{rem}} = (1.38, 1.41, 1.53, 1.53, .172, 1.86, 2.04) M_{\odot}$ for $M = (10, 11, 12, 13, 15, 18, 20) M_{\odot}$, respectively.

The M_{rem} is the baryon mass and is not the observable neutron star mass. The observed mass is about 10 percent smaller due to the general relativistic effect and called gravitational mass (see e.g., Ref. 65)). The conversion from baryon to gravitational mass depends on the EOS of nuclear matter. In Table II we show the gravitational mass, M_{g} , for the UU model in Ref. 66) using UV14+UVII EOS⁶⁷⁾ for nuclear matter.

5.1. Comparison with the observed mass

Here we compare the M_{g} of our models with observed neutron star (NS) masses. NS masses are most accurately determined when they are in double NS systems. In this case if two or more post-Keplerian parameters are obtained, NS masses are precisely determined (e.g., Ref. 68), 69)). In Table III we show the NS masses and errors for these stars. Interestingly the mass distribution has peak at $1.33 M_{\odot}$ with a small dispersion $0.06 M_{\odot}$. These stars may be considered to keep their birth mass,⁷⁰⁾ so they are suitable to compare with our results. NSs in binaries with high mass companions are also considered to roughly keep their birth mass. Ref.⁷⁰⁾ discussed that the most likely values of the central mass and dispersions for these NSs are $1.28 M_{\odot}$ and $0.24 M_{\odot}$, respectively.

First we note that lowest NS mass in the table is $M_{\text{g}} = 1.16 - 1.20 M_{\odot}$, and this is consistent with the lowest M_{g} model in the YU model $M = 10 M_{\odot}$. As described above this model may roughly correspond to the lightest Fe-core collapse supernovae. For a smaller mass star such as $M = 9.5 M_{\odot}$ or less, the star once forms a O-Ne degenerate core and its collapse may lead a weak supernova explosion.¹⁴⁾

In the calculation by Ref. 14), the remnant neutron star has $M_{\text{rem}} = 1.36 M_{\odot}$ or $M_{\text{g}} \simeq 1.23 M_{\odot}$. This seems to be larger than the observed minimum

Table IV. NS masses in double NS systems and errors. See references for Ref. 70) and therein.

Name	Mass (M_{\odot})	Error (M_{\odot})
J0737-3039	1.3381	0.0007
pulsar B	1.2489	0.0007
B1534+12	1.3332	0.0010
companion	1.3452	0.0010
J1756-2251	1.40	0.02
companion	1.18	0.02
J1906+0746	1.248	0.018
companion	1.365	0.018
B1913+16	1.4398	0.002
companion	1.3886	0.002
B2127+11C	1.358	0.010
companion	1.354	0.010

mass NS, though these O-Ne supernovae have not been studied well and currently only one progenitor model exists,^{71),72)} therefore we do not know the general properties of these SNe yet.

For the observed double NS typical mass range is $M_g = 1.27 - 1.39M_\odot$ as mentioned above. This corresponds to $M \sim 11.5 - 20M_\odot$ for UN model and $M \sim 12 - 14M_\odot$ for YU model.

Largest NS mass in the table is $M_g = 1.44M_\odot$ and this corresponds to $M \simeq 22M_\odot$ for the UN model, and $M \simeq 15M_\odot$ for the YU model. It is usually said that the border of NS and blackhole formation is at around $M = 20 - 25M_\odot$. Therefore it appears that the M_g range of the UN model is consistent with the double NS mass range, though we have not confirmed yet if the UN model with $M \lesssim 11M_\odot$ would result in $M_g \sim 1.2M_\odot$ NSs.

If we adopt the YU model, the mass range of double NS corresponds to rather narrow range, $M \sim 12 - 14M_\odot$, and it is difficult to understand the reason why. However at this moment we cannot say that the UN model represents the reality better, because the number of the double NS systems are still limited. In Ref. 70) using the model of Ref. 73) they also discussed that the narrow mass range of M_g in double NS systems are difficult to understand and suggested a particular and rare formation channel for the systems. On the other hand, the NS mass in binaries with high mass companion ranges $M_g = 1.04 - 1.52M_\odot$.⁷⁰⁾ Although this estimate is more uncertain than that in double NS systems, this wider range would be more easily understood in the YU model.

In summary NS mass observations would certainly provide interesting and important information to constrain the progenitor model, $X_C(^{12}\text{C})$ and $^{12}\text{C}(\alpha, \gamma)^{16}\text{O}$ rate. Interestingly all the observed NSs mentioned above have relatively small mass compared with the “recycled” NSs. NSs with white dwarf companions, millisecond pulsars and in low-mass X-ray binaries are called recycled and currently undergoing accretion. It is now known that these NS can surely be as massive as $M_g = 2.0M_\odot$ as the case for J1614-2230.⁷⁴⁾ Observations and theory are consistent in the sense that such massive NSs are rarely formed by the normal supernova explosions. Theoretically, when we fix the explosion energy, M_{rem} increases rapidly around $M \sim 25M_\odot$. This explains why massive NSs are rarely formed. It will be very interesting to constrain observationally that how massive NS can be formed at birth.

§6. Other recent works of our group

In this paper we have described our recent work on stellar evolution with some new results. Here we briefly review other works of our group not mentioned above.

6.1. (Magneto-)Hydrodynamical Simulations

T. Kuroda and H.U. have developed a 3D magnet-hydrodynamical general relativistic code with adaptive mesh refinements.⁷⁵⁾ This code was used to follow gravitational Fe core collapse and to calculate spectra of gravitational waves. We will apply this code to various progenitor models to explore explosion mechanism

and nucleosynthesis.

6.2. *Special Relativistic Hydrodynamical Simulations for GRB Jets*

S. Okita and H.U. have developed a 2D special relativistic hydrodynamical code. Using this code, Okita and H.U.⁷⁶⁾ explored the conditions for successful ejection of ultra-relativistic jets in the collapsar model of GRBs. This code is also applied to explore various aspects of explosions and nucleosynthesis in SNe and GRBs. One example is given in the next subsection.

6.3. *Evolution and nucleosynthesis in very massive stars which end up Fe core-collapse SNe*

Motivated by the discoveries of very luminous SNe, such as SN 1999as (SN Ic)⁷⁷⁾ and SN 2006gy (SN IIn),⁷⁸⁾ H.U. and K. Nomoto¹⁷⁾ calculated evolution of metal-poor massive stars in the mass range $M = 20 - 100 M_{\odot}$ with metallicity $Z = 10^{-4}$ to study how much ^{56}Ni is produced in core collapse SNe (CCSNe). They found that ^{56}Ni of $\sim 13 M_{\odot}$ can be produced for the $100 M_{\odot}$ star. This amount is sufficiently large to explain SN 1999as if the SN shines by the ^{56}Ni decay.

Since the actual bright SNe Ic usually appears in a host galaxy having metallicity larger than $Z = 10^{-4}$, mass-loss effect becomes important. Therefore, T. Y. & H.U.²⁰⁾ studied the uncertainties in mass-loss in detail for $Z = 0.004$ which corresponds to the host galaxy of SN 2007bi. SN 2007bi was a very bright SN Ic and $3.6 - 7.4 M_{\odot}$ of ^{56}Ni is required if it shines by radioactive ^{56}Ni . First Gal-Yam et al.⁷⁹⁾ discussed that the SN was a pair-instability SN (PISN) but Moriya et al.⁸⁰⁾ showed that they can be a CCSN if a $\sim 43 M_{\odot}$ CO star explodes with $E_{\text{exp}} = 3 \times 10^{52}$ erg.

Since PISN model is much more massive than the CCSN model, these models predicts quite different light curves. Unfortunately without the LC data well before the maximum light one could not distinguish these two models. T.Y. and H.U.²⁰⁾ found that for $Z = 0.004$, required ZAMS ranges are $M = 110 - 280 M_{\odot}$ and $M = 515 - 575 M_{\odot}$ for CCSN and PISN model, respectively. They provided that, if the progenitor was a single star and assuming the Salpeter's IMF, the ratio of the probabilities of CCSN to that of PISN appropriate for SN 2007bi is 42. We should remind, though, for the CCSN model we are assuming that such a large CO star can explode energetically. So far no one could have shown such a explosion from the first principle calculations.

Under the assumption that it can explode Okita, H. U., and T. Y. simulated spherically symmetric and axisymmetric jet-like core-collapse supernova explosions of a $M_{\text{f}} = 43.2 M_{\odot}$ WO star in Ref. 20).^{81), 82)} This progenitor is evolved from a $M = 110 M_{\odot}$ star with the metallicity of $Z = 0.004$. The CO core mass is $M_{\text{CO}} = 38.2 M_{\odot}$. For spherically symmetric calculations the same method as described in §4 is used. For the jet-like explosion the same code mentioned in §6.2 was used. After the explosion simulations, nucleosynthesis is calculated post-processingly. First we investigate the explosion-energy dependence of the ^{56}Ni amount. We found that ^{56}Ni larger than $3 M_{\odot}$, enough to reproduce the light curve of SN 2007bi, is produced in the supernova ejecta if the explosion energy is larger than 2×10^{52} erg. The

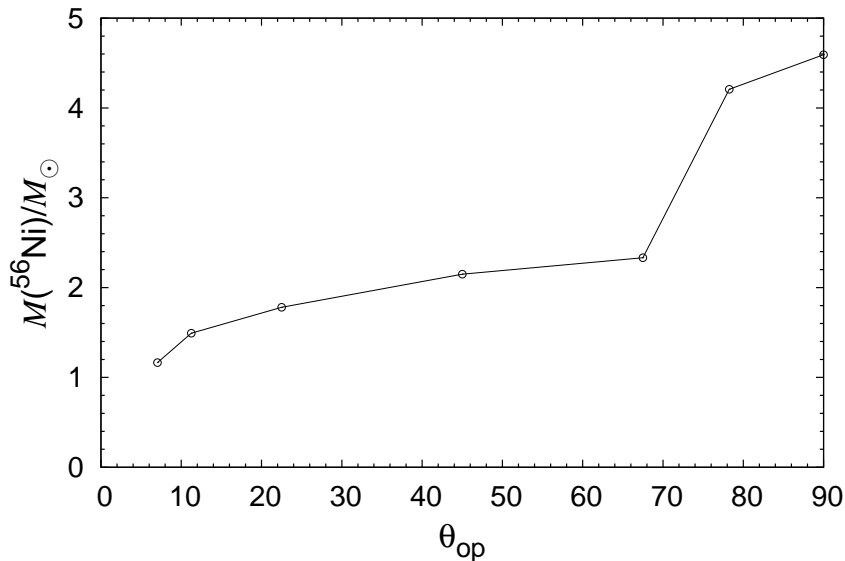


Fig. 14. The relation between the ejected ^{56}Ni amount and opening angle θ_{op} in axisymmetric supernova model. The progenitor is a $43.2 M_{\odot}$ WO star. The explosion energy is set to be 3×10^{52} erg.

investigation by the jet-like explosions with different opening angles θ_{op} with $E_{\text{exp}} = 3 \times 10^{52}$ erg indicated that the ejected ^{56}Ni yield strongly depends on the opening angle. Fig. 14 shows the relation between the amount of the ejected ^{56}Ni and the opening angle. Although the spherical explosion releases the amount of $4 M_{\odot}$ ^{56}Ni in the ejecta, the ejected ^{56}Ni is much smaller when the opening angle is smaller than 78° . The ejected amount of ^{56}Ni is smaller than $2.3 M_{\odot}$ for the opening angle smaller than 68° . This suggest that if SN 2007bi was a CCSN, it exploded with large opening angle or the explosion was more energetic than 3×10^{52} erg.

6.4. Pop III very massive stars: Evolution, Dark stars, Stability

The formation of first generation or Population (Pop) III stars in the Universe is considered to be quite different from that of later generation stars. This is because when the first generation stars were formed there was no metal yet, thus radiative feedback from the proto star was weak and might not be able to stop gas accretion. Also gas accretion rate itself was larger than the present universe. As a result it was expected that typical mass of Pop III stars were $100 M_{\odot}$ or more (e.g., Ref. 83)).

In Ohkubo, H.U. et al.,⁸⁴⁾ they calculated evolution and nucleosynthesis in the very massive 500 and $1000 M_{\odot}$ stars assuming that they explode energetically. Next, by taking account of a realistic mass accretion rate, Ref. 85) calculated Pop III star evolution with the mass accretion. They found that typically $500 - 1000 M_{\odot}$ stars were formed. It is notable that this mass range is larger than the often said mass range for a Pop III star, $M = 140 - 300 M_{\odot}$. If the mass range is in the $140 - 300 M_{\odot}$ range, most first stars should have exploded as PISNe. However, the abundance

patterns of EMP and HMP stars with $[\text{Fe}/\text{H}] < -4$ are not consistent with the yields of PISNe.¹⁶⁾

These works, however, neglected the effects on the accretion disk likely formed around the first stars. Ref. 86) and 87) investigated such effects and showed that the accretion disk was evaporated by the radiative feedback. Then the accretion onto a first star may stop before its mass grows more than $100 M_{\odot}$, preventing the formation of a PISN.⁸⁷⁾

Even though it is true, there is still a possibility for the formation of $1000 M_{\odot}$ stars. First stars are formed around the center of a dark halo where the density of dark matter is much higher than other places. Refs. 88), 89) showed that if the dark matter is self-annihilating WIMPs the self-annihilation energy is sufficiently large to sustain the first stars. Such stars are called “dark stars”. These stars typically have much larger radius, thus surface temperatures are lower and radiative feedback is expected to be weak. Hirano, H.U. and N. Yoshida⁹⁰⁾ calculated the dark star model with mass accretion. We confirmed that the stars keep large radius until it reaches the main sequence stage at around $M \sim 1000 M_{\odot}$.

H.U. et al.⁹¹⁾ also considered the accreting dark star model including the effects of captured dark matter annihilation that becomes important after the main sequence stage. They showed that if the baryon-dark matter scattering cross section is as large as $\sigma = 10^{-38} \text{cm}^2$, the dark stars could grow more: it could be 10^4 to $10^5 M_{\odot}$ depending on the mass accretion rates.

It has been known that such huge stars are vibrationally unstable against epsilon mechanism (e.g., Ref. 92)). As far as the star is sustained by the DM annihilation and not nuclear burning, the epsilon mechanism does not operate. However after the main sequence stage, nuclear burning soon dominates unless the captured dark matter effect is important. Sonoi and H.U.⁹³⁾ explored the stability of such very massive stars against the epsilon mechanism. They found that the amount of mass loss is less than 10 percent of the whole stellar mass.

6.5. Dust Formation in Supernovae

H.U. has been working also on dust formation in supernovae with T. Nozawa, T. Kozasa and collaborators. For example, Nozawa et al.⁹⁴⁾ calculated the dust yield for Pop III supernovae including CCSNe and PISNe, and showed that large amount of dust grains would be produced in the early universe by these SNe. Ref. 95) calculated the dust destruction by the reverse shock in a supernova remnant. The theory of dust formation was also applied to actual supernovae. Ref. 96) and 97) for SN 2006jc and Cas A supernova remnant, respectively, showed that the observed data are reasonably reproduced by the theory. It was also applied to SNe Ia.⁹⁸⁾ These dust grains in supernovae play important roles in the star and galaxy formation, and chemical evolution in the galaxies.

6.6. Presolar Grains from Supernovae

Presolar grains are recovered from primitive meteorites or interplanetary dusts and are identified as the grains having very large isotopic anomalies compared with the solar-system materials (e.g., reviews 99), 100)). Observed isotopic ratios of the

grains are considered to indicate the traces of the nucleosynthesis in stars at their birth or Galactic chemical evolution. Small amount of presolar grains are considered to originate from supernovae. They mainly indicate the excesses of ^{12}C , ^{15}N , and ^{28}Si . Some supernova grains show evidence for original presence of radioactive ^{44}Ti in Ca isotopic ratios, which strongly supports their origin. Isotopic ratios of heavy elements such as Mo and Ba have been also observed. However, it is still difficult to reproduce observed isotopic ratios by supernova models. Bulk composition of supernova ejecta of supernova models does not reproduce observed isotopic ratios of supernova grains.¹⁰¹⁾ In order to reproduce observed isotopic ratios, inhomogeneous mixing is required.

TY and Hashimoto¹⁰²⁾ and TY¹⁰³⁾ investigated supernova mixtures reproducing several isotopic ratios of supernova originating SiC and graphite grains. They divided supernova ejecta into seven different layers and investigated the mixing ratios reproducing C, N, O, Al, Si, and Ti isotopic ratios as many as possible for individual grains. The mixing ratios of the mixtures strongly depend on the reproduced isotopic ratios. The main component of the mixtures are the innermost Ni layer and the outer He/C and He/N layers, so that inhomogeneous mixing of supernova eject is necessary. TY, HU, and Nomoto¹⁰⁴⁾ investigated the supernova mixtures of different stellar masses reproducing Si isotopic ratios of supernova grains. They obtained that less massive supernovae with $M \lesssim 15M_{\odot}$ and hypernovae are preferable to reproducing Si isotopic ratios of supernova grains.

§7. Discussions and Future Prospects

7.1. Massive star evolution

In this paper we explained the differences in the newly developed efficient YU code and previous UN code, and shown that the YU code yields reasonable results as shown in §3 in some detail. We need such an efficient code because the study of massive star evolution still requires heavy amount of calculations as described in the followings.

As shown in Tables I and II, the results of UN and YU models presented in this paper are different mainly because $X_{\text{C}}(^{12}\text{C})$ is different. The values of $X_{\text{C}}(^{12}\text{C})$ sensitively depend on the $^{12}\text{C}(\alpha, \gamma)^{16}\text{O}$ rate and treatment of convection. Since it is currently not possible to determine the $^{12}\text{C}(\alpha, \gamma)^{16}\text{O}$ rate, we need calculate for various choices of the rate to find a best set to fit observations. Traditionally nucleosynthetic argument shown in §4.1 has given the most stringent constraint on $X_{\text{C}}(^{12}\text{C})$ and the $^{12}\text{C}(\alpha, \gamma)^{16}\text{O}$ rate. However, as shown in Fig. 11, it is not easy to distinguish even the UN and YU models because abundance data are only given for the IMF weighted yields.

We propose here that NS mass distribution will give alternative and independent constraints on the $X_{\text{C}}(^{12}\text{C})$ and $^{12}\text{C}(\alpha, \gamma)^{16}\text{O}$ rate. As shown in §5 and Table II, UN and YU models predict different mass distribution for the remnant NSs. Though the differences are not so large, observed NS masses are given in very fine precision for the double NS systems (Table IV). Therefore, by calculating stellar evolution in

binary systems, we may constrain the $X_C(^{12}\text{C})$ and $^{12}\text{C}(\alpha, \gamma)^{16}\text{O}$ rate more precisely, though it requires many calculations for various possible binary pairs.

One of our purposes for developing the efficient code is to tackle on the evolutions just below and above the Fe-core forming SNe. As mentioned in §3.1, such stars experience violent shell flashes near the end of their evolution. It is not clear yet if such events cause mass loss and shock interactions to be observable. In order to follow these stages precisely, it is important for a code to include the acceleration term. As mentioned in §2, we will include the term into the YU code in near future.

The stars just below the critical mass for the Fe-core formation is very interesting for another reason. Such a star may become an electron capture supernova (ECSN). We would like to construct another progenitor models of ECSNe than the one by Ref. 72) to see if the successful explosion by Ref. 14) is model independent or not. Since these calculations require high numerical resolution in both time and space,⁸⁾ we need an efficient code to perform computation.

We have been working also to develop a new code including the rotation effects as in Refs. 105), 106), 107), 108), 109), 110). This code is based on the YU code and aiming for efficient computation as well. Although rotating stellar models in the 1D formalism have been already calculated by these authors, angular momentum transfer is still quite uncertain. Therefore, the evolution of a rotating star is still far from complete understanding. Since rotation is inevitable for constructing realistic progenitor models for hypernovae and GRBs, and possibly even for normal CCSNe, we plan to calculate rotating progenitor models as well.

The uncertainties in mass-loss rate is the another reason why one needs to compute several cases to find a better set. Since the knowledge for the rate is still very limited, one needs to constrain the rate by using various information including the properties of massive stars, supernovae, compact remnants, ISM abundances and so on. Unfortunately this may not be easy because other uncertain factors may be involved such as rotation, binarity and magnetic field effects. Supernovae may provide a key to understand the rate. For example, as discussed in Ref. 20) if one can identify SN 2007bi-like event to a CCSN or PISN, we can severely constrain the mass loss rates.

7.2. Nucleosynthesis

As for our nucleosynthetic works, in §4 we described the success and limitations of the simple 'instant energy injection' model. This model reasonably reproduce supernova yields up to Zn. Although spherically symmetric hypernova models over-produce Fe to lighter elements ratio, such as Fe/O, this problem may be avoided if one consider jet-like explosions in 2D for hypernovae even under the instant energy injection model. This suggests that the nucleosynthesis up to Zn does not much depend on the detail of the central engine.

On the other hand, nucleosynthesis of r- and weak r-process elements depends on the detail of the explosion model. This in turn implies that successful supernova and/or hypernova and/or GRB models must produce these elements.

As described in Ref. 40) there are observational indications that normal CCSNe produce lighter weak r-process elements, Sr, Y and Zr. These elements can be

produced and ejected from the hot bubble of normal SNe. However, to produce heavier weak r-process elements, Mo and Ru, much larger entropy and neutron rich environment is required.⁵⁶⁾ It is currently not certain if such an environment can be realized in a CCSN. This is because long term simulations of a CCSN showed that high-entropy matter ejected from a CCSN is always almost neutral or proton-rich.⁶¹⁾ As mentioned in §4, it is not clear if all Sr-Zr rich EMP stars are also Mo-Ru rich. If this is the case, a CCSN model has to produce Mo-Ru somehow. One possibility is the νp -process (Refs. 111), 112), 113), 114)) not considered in Ref. 56). With this process, such weak r-process elements may be synthesized in proton-rich matter if entropy is sufficiently high. Thus it is critically important to observationally clarify if normal SNe produce Mo-Ru or not. We should note that the results in Ref. 61) are not obtained by the first principle calculations, but the explosion is driven by artificially enhancing the effective neutrino luminosity. The main reason that the matter becomes proton-rich is because of the interaction between matter and neutrino. If the explosion is driven by the assist of something else, such as the rotation energy, neutron rich matter may be ejected.

The arguments above also applies to the r-process elements. Currently there is no clear evidence in the EMP stars that r-process elements are produced in normal CCSNe and hypernovae. For example, Zn-rich EMP stars, that we consider them polluted by a hypernova, show no enhancement of r-process elements. From the results in Ref. 61), it seems hopeless to produce r-process elements in normal CCSNe, though unknown massive stars should have polluted metal poor r-rich stars, such as CS22892-052. Some authors consider NS-NS or NS-blackhole merger systems for r-process sites (e.g., Refs. 115), 116), 117), 118), 119), 120)) though it is not clear yet if such sites are sufficient to explain the whole r-process abundance in the universe. Therefore it is still interesting to explore various SN explosion models to examine if they can produce r-process elements or not.

Acknowledgements

We thank Hideyuki Saio for providing the stellar evolution code and useful comments. We are grateful to K. Nomoto and S. Okita for useful discussions. We acknowledge support by the grants-in-aid for Scientific Research (20041005, 20105004) from the MEXT of Japan.

References

- 1) S. J. Smartt, *Ann. Rev. Astron. Astrophys.* **47** (2009), 63.
- 2) M. Herant, W. Benz, W. R. Hix, C. L. Fryer and S. A. Colgate, *Astrophys. J.* **435** (1994), 339.
- 3) J. M. Blondin, A. Mezzacappa and C. DeMario, *Astrophys. J.* **584** (2003), 971.
- 4) K. Kotake, H. Sawai, S. Yamada and K. Sato, *Astrophys. J.* **608** (2004), 391.
- 5) A. Burrows, E. Livne, L. Dessart, C. D. Ott and J. Murphy, *Astrophys. J.* **640** (2006), 878.
- 6) N. Ohnishi, K. Kotake and S. Yamada, *Astrophys. J.* **641** (2006), 1018.
- 7) T. Takiwaki, K. Kotake and Y. Suwa, *Astrophys. J.* **749** (2012), 98.
- 8) A. J. T. Poelarends, F. Herwig, N. Langer and A. Heger, *Astrophys. J.* **675** (2008), 614.
- 9) S. E. Woosley, A. Heger and T. A. Weaver, *Rev. Mod. Phys.* **74** (2002), 1015.

- 10) H. Umeda, K. Nomoto, H. Yamaoka and S. Wanajo, *Astrophys. J.* **513** (1999), 861.
- 11) S. E. Woosley and T. A. Weaver, *Ann. Rev. Astron. Astrophys.* **24** (1986), 205.
- 12) K. Nomoto and M. Hashimoto, *Phys. Rep.* **163** (1988), 13. (NH88)
- 13) S. Miyaji, K. Nomoto, K. Yokoi and D. Sugimoto, *Publ. Astron. Soc. Jpn.* **32** (1980), 303.
- 14) F. S. Kitaura, H.-Th., Janka, W. Hillebrandt, *Astron. and Astrophys.* **450** (2006), 345.
- 15) S. E. Woosley and T. A. Weaver, *Astrophys. J. Suppl.* **101** (1995), 181.
- 16) H. Umeda and K. Nomoto, *Astrophys. J.* **565** (2002), 385.
- 17) H. Umeda and K. Nomoto, *Astrophys. J.* **673** (2008), 1014.
- 18) A. Chieffi and M. Limongi, *Astrophys. J.* **502** (1998), 737.
- 19) A. Heger, S. E. Woosley, G. Mart  nez-Pinedo and K. Langanke, *Astrophys. J.* **560** (2001), 307.
- 20) T. Yoshida and H. Umeda, *Mon. Not. R. Astron.* **412** (2011), L78.
- 21) H. Umeda and K. Nomoto, *Nature* **422** (2003), 871.
- 22) H. Umeda and K. Nomoto, *Astrophys. J.* **619** (2005), 427.
- 23) H. Saio, K. Nomoto and M. Kato, *Astrophys. J.* **331** (1988), 388.
- 24) R. Kippenhahn and A. Weigert, *Stellar Structure and Evolution*, Study edition, (A&A Library: Springer-Verlag, 1990).
- 25) H. C. Spruit, *Astron. and Astrophys.* **253** (1992), 131.
- 26) W. Unno, *Publ. Astron. Soc. Jpn.* **19** (1967), 140.
- 27) K. Nomoto and D. Sugimoto, *Publ. Astron. Soc. Jpn.* **29** (1977), 765.
- 28) J. S. Vink, A. de Koter and H. J. G. L. M. Lamers, *Astron. and Astrophys.* **369** (2001), 574.
- 29) C. de Jager, H. Nieuwenhuijzen and K. A. van der Hucht, *Astron. and Astrophys. Suppl.* **369** (1988), 574.
- 30) R. Kudritzki, A. Rauldrach, J. Puls and D. Abbott, *Astron. and Astrophys.* **219** (1989), 205.
- 31) T. A. Weaver and S. E. Woosley, *Phys. Rep.* **227** (1993), 65.
- 32) G. A. Caughlan and W. A. Fowler, *At. Data Nucl. Data Tables* **40** (1988), 283. (CF88)
- 33) G. A. Caughlan, W. A. Fowler, M. Harris, and B. Zimmerman, *At. Data Nucl. Data Tables* **32** (1985), 197.
- 34) N. Tominaga, H. Umeda and K. Nomoto, *Astrophys. J.* **660** (2007), 516.
- 35) L. Buchmann, *Astrophys. J.* **468** (1996), L127.
- 36) R. Kunz, M. Fey, M. Jaeger, A. Mayer, J. W. Hammer, G. Staudt, S. Harissopulos and T. Paradellis, *Astrophys. J.* **567** (2002), 643.
- 37) K. Takahashi, H. Umeda and T. Yoshida, *Death of Massive Stars: Supernovae & Gamma-Ray Bursts*, Proceedings of the IAU Symposium **279** (2012), in press.
- 38) T. Yoshida, H. Umeda and K. Nomoto, *Astrophys. J.* **672** (2008), 1043.
- 39) F.-K. Thielmann, K. Nomoto and M. Hashimoto, *Astrophys. J.* **460** (1996), 408.
- 40) N. Izutani, H. Umeda and N. Tominaga, *Astrophys. J.* **692** (2009), 1517.
- 41) S. E. Woosley, D. H. Hartmann, R. D. Hoffman and W. C. Haxton, *Astrophys. J.* **356** (1990), 272.
- 42) T. Yoshida, M. Terasawa, T. Kajino and K. Sumiyoshi, *Astrophys. J.* **600** (2004), 204.
- 43) T. Yoshida, T. Kajino and D. H. Hartmann, *Phys. Rev. Lett.* **94** (2005), 231101.
- 44) T. Yoshida, T. Kajino, H. Yokomakura, K. Kimura, A. Takamura and D. H. Hartmann, *Phys. Rev. Lett.* **96** (2006), 091101.
- 45) T. Yoshida, T. Kajino, H. Yokomakura, K. Kimura, A. Takamura and D. H. Hartmann, *Astrophys. J.* **649** (2006), 319.
- 46) T. Yoshida, T. Suzuki, S. Chiba, T. Kajino, H. Yokomakura, K. Kimura, A. Takamura and D. H. Hartmann, *Astrophys. J.* **686** (2008), 448.
- 47) T. Suzuki, M. Honma, K. Higashiyama, T. Yoshida, T. Kajino, T. Otsuka, H. Umeda, and K. Nomoto, *Phys. Rev. C* **79** (2009), 061603.
- 48) K. Nakamura, T. Yoshida, T. Shigeyama and T. Kajino, *Astrophys. J. Lett.* **718** (2010), L137.
- 49) C. Kobayashi, N. Izutani, A. I. Karakas, T. Yoshida, D. Yong and H. Umeda, *Astrophys. J.* **739** (2011), L57.
- 50) N. Izutani, H. Umeda and T. Yoshida, *Death of Massive Stars: Supernovae & Gamma-Ray Bursts*, Proceedings of the IAU Symposium **279** (2012), in press.
- 51) C. Kobayashi, H. Umeda, K. Nomoto, N. Tominaga and T. Ohkubo, *Astrophys. J.* **653**

- (2006), 1145.
- 52) R. Cayrel et al. *Astron. Astrophys.* **416** (2004), 1117
 - 53) N. Tominaga, K. Maeda, H. Umeda, K. Nomoto, M. Tanaka, N. Iwamoto, T. Suzuki and P. A. Mazzali, *Astrophys. J.* **657** (2007), L77.
 - 54) K. Maeda et al., *Science* **319** (2008), 1220.
 - 55) A. Heger and S. E. Woosley, *Astrophys. J.* **724** (2010), 341.
 - 56) N. Izutani and H. Umeda, *Astrophys. J.* **720** (2010), 1.
 - 57) C. Sneden et al. *Astrophys. J.* **591** (2003), 936.
 - 58) S. Honda, W. Aoki, Y. Ishimaru and S. Wanajo, *Astrophys. J.* **666** (2007), 1189.
 - 59) R. Buras, M. Rampp, H.-Th. Janka and K. Kifonidis, *Astron. Astrophys.* **447** (2006), 1049.
 - 60) A. Marek and H.-Th. Janka, *Astrophys. J.* **694** (2009), 664.
 - 61) T. Fischer, S. C. Whitehouse, A. Mezzacappa, F.-K. Thielemann, and M. Liebendörfer, *Astron. Astrophys.* **517** (2010), 80.
 - 62) H.-Th. Janka, R. Buras and M. Rampp, *Nucl. Phys. A* **718** (2003), 269.
 - 63) T. Shigeyama, K. Nomoto and M. Hashimoto, *Astron. Astrophys.* **196** (1988), 141.
 - 64) K. Nomoto, M. Tanaka, N. Tominaga and K. Maeda, *New Astronomy Reviews* **54** (2010), 191.
 - 65) K. Nomoto and S. Tsuruta, *Astrophys. J.* **312** (1987), 711.
 - 66) H. Umeda, S. Tsuruta and K. Nomoto, *Astrophys. J.* **433** (1994), 256.
 - 67) R. B. Wiringa, V. Fiks and A. Fabrocini, *Phys. Rev. C* **38** (1988), 1010.
 - 68) L. S. Finn, *Phys. Rev. Lett.* **73** (1994), 1878.
 - 69) S. E. Thorsett and D. Chakrabarty, *Astrophys. J.* **512** (1999), 288.
 - 70) F. Ozel, D. Psaltis, R. Narayan and A. S. Villarreal, arXiv:1201.1006, (2012).
 - 71) K. Nomoto, *Supernova Remnants and their X-Ray Emission*, Proceedings of the IAU Symposium **101** (1983), 139.
 - 72) K. Nomoto, *Astrophys. J.* **277** (1984), 791.
 - 73) F. X. Timmes, S. E. Woosley and T. A. Weaver, *Astrophys. J.* **457** (1996), 834.
 - 74) P. B. Demorest, T. Pennucci, S. M. Ransom, M. S. E. Roberts and J. W. T. Hessels, *Nature* **467** (2010), 1081.
 - 75) T. Kuroda and H. Umeda, *Astrophys. J. Suppl.* **191** (2010), 439.
 - 76) S. Okita and H. Umeda, *Astrophys. J.*, submitted.
 - 77) J. S. Deng, K. Hatano, T. Nakamura, K. Maeda, K. Nomoto, P. Nugent, G. Aldring and D. branch, *New Century of X-ray Astronomy*, AIP Conf. Proc., **251** (2001), 238.
 - 78) E. O. Ofek et al. *Astrophys. J. Lett.* **659** (2007), L13.
 - 79) A. Gal-Yam et al. *Nature* **462** (2009), 624.
 - 80) T. Moriya, N. Tominaga, M. Tanaka, K. Maeda and K. Nomoto, *Astrophys. J.* **717** (2010), L83.
 - 81) T. Yoshida and H. Umeda, *Proceedings of the 11th International Symposium on Origin of Matter and Evolution of Galaxies*, AIP Conf. Proc., in press.
 - 82) S. Okita, H. Umeda and T. Yoshida, *Proceedings of the 11th International Symposium on Origin of Matter and Evolution of Galaxies*, AIP Conf. Proc., in press.
 - 83) N. Yoshida, L. Hernquist and N. Sugiyama, *Astrophys. J.* **592** (2003), 645.
 - 84) T. Ohkubo, H. Umeda, K. Maeda, K. Nomoto, T. Suzuki, S. Tsuruta and M. J. Rees, *Astrophys. J.* **645** (2006), 1352.
 - 85) T. Ohkubo, K. Nomoto, H. Umeda, N. Yoshida and S. Tsuruta, S., *Astrophys. J.* **706** (2009), 1184.
 - 86) C. F. McKee and J. C. Tan, *Astrophys. J.* **681** (2008), 771.
 - 87) T. Hosokawa, K. Omukai, N. Yoshida and H. W. Yorke, *Science* **334** (2011), 1250.
 - 88) D. Spolyar, K. Freese and P. Gondolo, *Phys. Rev. Lett.* **100** (2008), 1101.
 - 89) D. Spolyar, P. Bodenheimer, K. Freese and P. Gondolo, *Astrophys. J.* **705** (2009), 1031.
 - 90) S. Hirano, H. Umeda and N. Yoshida, *Astrophys. J.* **736** (2011), 58.
 - 91) H. Umeda, N. Yoshida, K. Nomoto, S. Tsuruta, M. Sasaki and T. Ohkubo, *J. Cosmo. Astropart. Phys.* **08** (2009), 024.
 - 92) I. Baraffe, A. Heger and S. E. Woosley, *Astrophys. J.* **550** (2001), 890.
 - 93) T. Sonoi and H. Umeda, *Mon. Not. R. Astron.* **421** (2012), L34.
 - 94) T. Nozawa, T. Kozasa, H. Umeda, K. Maeda and K. Nomoto, *Astrophys. J.* **598** (2003), 785.

- 95) T. Nozawa, T. Kozasa, A. Habe, E. Dwek, H. Umeda, N. Tominaga, K. Maeda and K. Nomoto, *Astrophys. J.* **666** (2007), 955.
- 96) T. Nozawa et al., *Astrophys. J.* **684** (2008), 1343.
- 97) T. Nozawa, T. Kozasa, N. Tominaga, K. Maeda, H. Umeda and K. Nomoto, *Astrophys. J.* **713** (2010), 356.
- 98) T. Nozawa, K. Maeda, T. Kozasa, M. Tanaka, K. Nomoto and H. Umeda, *Astrophys. J.* **736** (2011), 45.
- 99) E. Zinner, *Annu. Rev. Earth Planet. Sci.* **26** (1998), 147.
- 100) D. D. Clayton and L. R. Nittler, *Annu. Rev. Astron. Astrophys.* **42** (2004), 39.
- 101) C. Travaglio, R. Gallino, S. Amari, E. Zinner, S. Woosley, and R. S. Lewis, *Astrophys. J.* **510** (1999), 325.
- 102) T. Yoshida and M. Hashimoto, *Astrophys. J.* **606** (2004), 592.
- 103) T. Yoshida, *Astrophys. J.* **666** (2007), 1048.
- 104) T. Yoshida, H. Umeda, and K. Nomoto, *Astrophys. J.* **631** (2005), 1039.
- 105) A. Heger, N. Langer and S. E. Woosley, *Astrophys. J.* **528** (2000), 368.
- 106) R. Hirschi, G. Meynet and A. Maeder, *Astron. Astrophys.* **425** (2004), 649.
- 107) A. Heger, S. E. Woosley and H. C. Spruit, *Astrophys. J.* **626** (2005), 350.
- 108) S.-C. Yoon and N. Langer, *Astron. Astrophys.* **443** (2005), 643.
- 109) S. E. Woosley and A. Heger, *Astrophys. J.* **637** (2006), 914.
- 110) P. Eggenberger, G. Meynet, A. Maeder, R. Hirschi, C. Charbonnel, S. Talon and S. Ekström, *Astrophys. Space Sci.* **316** (2008), 43.
- 111) J. Pruet, S. E. Woosley, H.-T. Janka, R. Buras and R. D. Hoffman, *Astrophys. J.* **623** (2005), 325.
- 112) C. Fröhlich et al., *Astrophys. J.* **637** (2006), 415.
- 113) S. Wanajo, *Astrophys. J.* **647** (2006), 1323.
- 114) S. Wanajo, H.-Th. Janka and S. Kubono, *Astrophys. J.* **729** (2011), 46.
- 115) C. Freiburghaus, S. Rosswog and F.-K. Thielemann, *Astrophys. J. Lett.* **525** (1999), L121.
- 116) R. Surman, G. C. McLaughlin, M. Ruffert, H.-Th. Janka and W. R. Hix, *Astrophys. J.* **679** (2008), L117.
- 117) B. D. Metzger, A. L. Piro and E. Quataert, *Mon. Not. R. Astron.* **396** (2009), 304.
- 118) S. Goriely, A. Bauswein and H.-Th. Janka, *Astrophys. J.* **738** (2011), L32.
- 119) O. L. Caballero, G. C. McLaughlin and R. Surman, *Astrophys. J.* **745** (2012), 170.
- 120) S. Wanajo and H.-Th. Janka, *Astrophys. J.* **746** (2012), 180.